THE ELECTRICAL PROPERTIES OF EVAPORATED SILICON FILMS

by

TREVOR WILLIAM TUCKER

B.A.Sc., University of British Columbia, 1964

A THESIS SUBMITTED IN PARTIAL FULFILMENT OF

THE REQUIREMENTS FOR THE DEGREE OF

MASTER OF APPLIED SCIENCE

in the Department

of

Electrical Engineering

We accept this thesis as conforming to the

required standard

THE UNIVERSITY OF BRITISH COLUMBIA

July, 1966

In presenting this thesis in partial fulfilment of the requirements for an advanced degree at the University of British Columbia, I agree that the Library shall make it freely available for reference and study. I further agree that permission for extensive copying of this thesis for scholarly purposes may be granted by the Head of my Department or by his representatives. It is understood that copying or publication of this thesis for financial gain shall not be allowed without my written permission.

Department of Elec Eng

The University of British Columbia
Vancouver 8, Canada

Date 19 Aug 1966

ABSTRACT

The Hall coefficient and conductivity of silicon films vacuum deposited on 0° and 60° sapphire at $850^{\circ}C$ to $1050^{\circ}C$ were measured from $100^{\circ}K$ to $550^{\circ}K$. Films made from 0.094 Ω-cm p type and 1 Ω-cm n type silicon sources were prepared by electron bombardment heating of the source in a vacuum of 5×10^{-7} to 10^{-6} torr. The orientation and crystallinity of the films were investigated using electron diffraction.

It was found that defects in the films introduced both donor and acceptor levels. The heavy compensation thus produced in films deposited at lower temperatures lead to a very low hole concentration. All films were p type at room temperature showing that the acceptor levels slightly dominated the donor levels. The films deposited on 0° sapphire indicated fewer defects than those deposited on 60° sapphire. At high temperature ($> 950^{\circ}C$) doping of the silicon by aluminum atoms from the substrate was appreciable.

The Hall mobility of the films made from the p type source material decreased with increasing temperature of deposition. This apparent anomaly is explained by the use of the polycrystalline film model suggested by Volger (1950).

TABLE OF CONTENTS

		Page
LIST OF ILLUSTRATIONS		v
ACKNOWLEDGEMENT		viii
LIST OF SYMBOLS		ix
1.	INTRODUCTION	1
2.	THE GROWTH AND STRUCTURE OF FILMS AND THE EFFECT OF STRUCTURE ON THE ELECTRICAL PROPERTIES	3
	2.1 Structure of Films	3
	2.1.1 Film Growth	3
	2.1.2 Overgrowth Defects	4
	2.2 Electrical Properties	6
	2.2.1 Bulk Material	6
	2.2.2 Thin Films	13
3.	EXPERIMENTAL PROCEDURE AND APPARATUS	21
	3.1 Preparation of Films	21
	3.1.1 Description of the Vacuum System	21
	3.1.2 Preparation of Substrate and Source	22
	3.1.3 Evaporation Procedure	23
	3.2 Electrical Measurements	24
	3.2.1 Description of Circuit	25
	3.2.2 Accuracy of Measurement	28
	3.2.3 Specimen Holder and Heating/Cooling System	28
	3.2.4 The Specimen	29
	3.3 Electron Diffraction	32
4.	FILM GROWTH AND STRUCTURE	34
	4.1 Effect of Rate of Arrival of Vapour Atoms on Growth of Initial Grains	34
	4.2 Growth of Film after Becoming Continuous	35
	4.3 Effect of Microscratches on the Substrate	36
	4.4 Variation of Crystallite Dimensions with Substrate Temperature and Orientation	37
	4.5 Effect of Lattice Orientation in the Substrate	38
5.	ELECTRICAL PROPERTIES	42
	5.1 Effect of Film Thickness	42
	5.2 General Discussion	46
	5.3 Effect of Temperature of Deposition	50
	5.4 Effect of the Nature of the Substrate	56

Page

5.4.1 Substrate Orientation (Al_2O_3) 56
5.4.2 Other Substrate Materials 61
5.5 Reproducibility of Electrical Properties 62
5.6 Homogeneity of Films 66

6. CONCLUSIONS 71

APPENDIX I
THE VAN DER PAUWCONFIGURATION 73

REFERENCES 75

LIST OF ILLUSTRATIONS

Figure		Page
1	Schematic Representation of Interfacial Dislocations	5
2	Variation of Hole Concentration with Temperature in a Typical Semiconductor	8
3	Representation of a Dislocation	11
4	Effect of Surface States on the Energy Bands .	14
5	Band Bending Caused by Grain Boundaries	15
6	The Inhomogeneous Film Model	16
7	Resistive Analogue of Inhomogeneous Film Model	17
8	Hall Voltage Analogue of Inhomogeneous Film Model	18
9	Shorting Effect of Contacts on the Hall Coefficient	19
10	The Evaporation System	23
11	The Hall Effect Apparatus	25
12	Circuit of Hall Effect Apparatus	26
13	The Specimen Holder	27
14	A Substrate Showing Three Specimens	30
15	Photomicrograph of the Growth of Initial Grains (at 950°C on 0° Sapphire)	34
16	Photomicrograph of Film 0.1μ Thick Deposited 950°C on to 60° Sapphire	35
17	Diffraction Patterns of Films of Various Thickness Deposited at 950°C on to 60° Sapphire	36
18	Photomicrograph of a Film Grown at 1060°C on 0° Sapphire Showing Preferred Nucleation at Microscratches	36
19	Photomicrographs of Films Deposited on 0° Sapphire at Various Temperatures	37
20	Variation of Average Crystallite Size with Temperature ofDeposition	38

Figure		Page
21	Electron Diffraction Patterns of Films Deposited on 60° Sapphire at Various Temperatures	39
22	Electron Diffraction Patterns of Films Deposited on 0° Sapphire at Various Temperatures	39
23	Variation of Average Growth Rate of Film with Temperature of Deposition	41
24	Resistivity vs. Temperature for Films of Various Thicknesses Deposited at 950°C on to 60° Sapphire from a p type Source	43
25	Hole Concentration vs. Temperature for Films of Various Thicknesses Deposited at 950°C on to 60° Sapphire from a p type Source	44
26	Hall Mobility vs. Temperature for Films of Various Thicknesses Deposited at 950°C on to 60° Sapphire from a p type Source	45
27	Hole Concentration vs. Temperature Showing Effect of the Degree of Compensation	48
28	Resistivity vs. Temperature for Films Deposited on to 0° Sapphire at Various Temperatures from n and p type Sources	51
29	Hall Coefficient vs. Temperature of Films Deposited on to 0° Sapphire at Various Temperatures from n and p type Sources	52
30	Hall Mobility vs. Temperature for Films Deposited on to 0° Sapphire at Various Temperatures from n and p type Sources	53
31	Conductivity vs. Temperature for Films Deposited on to 0° and 60° Sapphire at Various Temperatures from a p type Source	57
32	Hole Concentration vs. Temperature for Films Deposited on to 0° and 60° Sapphire at Various Temperatures from a p type Source	58
33	Hall Mobility vs. Temperature for Films Deposited on to 0° and 60° Sapphire at Various Temperatures from a p type Source	59
34	Conductivity vs. Temperature for Two Films Deposited on to 60° Sapphire at 950°C from a p type Source	63

Figure		Page
35	Hole Concentration vs. Temperature for Two Films Deposited on to 60° Sapphire at 950°C from a p type Source	64
36	Hall Mobility vs. Temperature for Two Films Deposited on to 60° Sapphire at 950°C from a p type Source	65
37	Electron Diffraction Patterns of Two Films Deposited at 950°C on 60° Sapphire	66
38	Conductivity vs. Temperature for Three Specimens Deposited on to a 0° Sapphire Substrate at 950°C from an n type source	67
39	Hall Coefficient vs. Temperature for Three Specimens Deposited on to a 0° Sapphire Substrate at 950°C From an n type Source ...	68
40	Hall Mobility vs Temperature for Three Specimens Deposited on to a 0° Sapphire Substrate at 950°C from an n type Source	69

ACKNOWLEDGEMENT

The author is indebted to Dr. L. Young for his help and guidance throughout the course of this investigation. Grateful acknowledgement is also given to Dr. J.S. MacDonald for reading the manuscript and for his helpful suggestions.

The author is grateful to Mr. C.A.T. Salama for many helpful discussions, to Mr. N. Owen for assistance in the design and construction of the Hall effect apparatus, to Messrs. A. Horn, R. Proudlove, A. MacKenzie, I. Huff, and H. Stuber for their technical help, to Dr. F. Murray of the B.C. Research Council for the use of the Cary spectrophotometer, to Miss B. Rydberg for typing the thesis, and to Messrs. G. Teather and G. Yan for proof reading the manuscript.

Grateful acknowledgement for financial support is given to the National Research Council (Block Term Grant A68) and to the Defence Research Board (contract ECRDC T65A).

The work described in this thesis was supported by the Defence Research Board under contract ECRDC T65A and by the National Research Council under Grant A-68. The electron microscope was provided by the National Research Council under major equipment grant E-680.

LIST OF SYMBOLS

p - hole concentration (holes/cm^3)

N_D - concentration of donor states (states/cm^3)

n_D - concentration of unionized donor states (states/cm^3)

n - electron concentration (electrons/cm^3)

N_A - concentration of acceptor states (states/cm^3)

p_A - concentration of unionized acceptor states (states/cm^3)

m_p - effective mass of holes (grams)

k - Boltzmann's constant = 1.37×10^{-16} erg/^oK

T - absolute temperature (^oK)

h - Planck's constant = 6.55×10^{-27} erg-sec

$\hbar$ - $h/2\pi$

E_F - Fermi energy (ev)

E_v - potential energy of the top of valence band (ev)

E_D - potential energy of a donor level (ev)

E_A - potential energy of an acceptor level (ev)

σ - conductivity $(\text{ohm-cm})^{-1}$

$\rho = \frac{1}{\sigma}$ - resistivity (ohm-cm)

q - magnitude of electronic charge = 1.6×10^{-19} coul

μ_n - mobility of electrons (cm^2/v-sec)

μ_p - mobility of holes (cm^2/v-sec)

μ_l - portion of the hole mobility due to lattice scattering (cm^2/v-sec)

d - density (gm/cm^3)

u_l - velocity of long compressional waves in the crystal (cm/sec)

E_l - energy associated with the perturbation of the lattice atom (ergs)

μ_u - portion of the hole mobility due to uncharged impurity scattering (cm^2/v-sec)

a_1 - $\frac{m}{m_p}\frac{\varepsilon}{\varepsilon_o}\ a_o$

m - mass of an electron in free space = 9.03×10^{-28} grams

N_n - concentration of neutral impurities (cm^{-3})

ε_o - permittivity of free space = 8.854×10^{-12} farad/m

ε - permittivity (farad/m)

K - relative dielectric constant = $\varepsilon/\varepsilon_o$

a_o - radius of Bohr orbit = 5.29×10^{-9} cm

μ_{IN} - portion of the hole mobility due to charge impurity (non-degenerate) scattering

N_I - concentration of charged impurities (cm^{-3})

Z - the difference in valency between impurity atoms and bulk material

A_H - Hall coefficient (cm^3/coul)

α - μ_H/μ_p

μ_H - Hall mobility (cm^2/v-sec)

γ - μ_n/μ_p

L_D - Debye Length (cm)

l_1 - length of the crystallites in the inhomogeneous film model (cm)

l_2 - width of the grain boundaries in the inhomogeneous film model (cm)

ρ_1 - resistivity of the crystallites (Ω-cm)

ρ_2 - resistivity of the grain boundaries (Ω-cm)

$\bar{A}_H$ - Hall coefficient of the inhomogeneous film (cm^3/coul)

A_{H1} - $\frac{1}{p_1 q}$

A_{H2} - $\frac{1}{p_2 q}$

p_1 - hole concentration in the crystallites of inhomogeneous film model (holes/cm^3)

p_2 - hole concentration in grain boundaries of inhomogeneous film model (holes/cm^3)

μ_1 - hole mobility in crystallites of inhomogeneous film model (cm^2/v-sec)

μ_2 - hole mobility in grain boundaries of inhomogeneous film model (cm^2/v-sec)

R_3 - resistance of a grain boundary in the inhomogeneous film model which lies parallel to the length of the specimen and is $(l_1 + l_2)$cm long (ohms)

R_1 - resistance of a crystallite in the inhomogeneous film model (ohms)

R_2 - resistance of a grain boundary in the inhomogeneous film model which lies perpendicular to the length of the specimen and is l_1 cm long (ohms)

$\bar{R}$ - total resistance of inhomogeneous film model (Ω)

t - thickness of the film (cm)

N - number of crystallites in the length of the specimen in the inhomogeneous film model

n - number of crystallites in the width of the specimen in the inhomogeneous film model

$\bar{A}_H$ - Hall coefficient of inhomogeneous film model (cm^3/coul)

$\bar{V}_H$ - Hall voltage of inhomogeneous film model (volts)

B - magnetic flux density (webers/m^2 in mks, gauss in esu)

V_1 - Hall voltage produced by the crystallite of the inhomogeneous film model (volts)

V_2 - Hall voltage produced by the grain boundaries which lie parallel to the length of the specimen (volts)

V_3 - Hall voltage produced by the grain boundaries which lie perpendicular to the length of the specimen (volts)

I_t - total current passing through the film (amps)

c - coefficient resulting from the tendency of low resistance contacts to short the Hall voltage in short, wide specimens

$\bar{p}$ - $\frac{1}{\bar{A}_H q}$ effective hole concentration in the inhomogeneous film model (cm^{-3})

μ_{Heff} - $\bar{A}_H/\bar{\rho}$ effective Hall mobility of holes in the inhomogeneous film model ($cm^2/v\text{-}sec$)

1. INTRODUCTION

The purpose of the work which is reported in this thesis was to investigate the electrical properties of thin films of silicon prepared by vacuum evaporation and to relate these properties to the structure of the films and the doping of the source material. The structure, in turn, was related to the conditions under which growth of the films occurred.

The structure of the films is affected by the material comprising the substrate and by the orientation of the substrate. Films deposited on CaF_2, MgO, and on two different orientations of α-Al_2O_3 were examined. Film structure is also influenced by the temperature of the substrate during deposition, hence films deposited on Al_2O_3 at several different temperatures were examined.

The electrical properties of films fabricated from n type and p type silicon were tested. The effect of the thickness on the electrical properties was also investigated.

Examination of the electrical properties consisted of measuring the conductivity and Hall coefficient of each specimen over the temperature range of 100°K to 550°K. For single crystal material, such data gives the type, concentration, and mobility of the majority carriers. As will be shown, the interpretation of macroscopic conductivity and Hall coefficient is more complicated for polycrystalline material than for single crystal bulk material.

In recent years there has been an increasing amount of effort expended on studies of semiconducting films deposited on to both insulating and semiconducting substrates. Such films

are being studied because they are useful in integrated circuits. Of the group IV semiconductors (germanium and silicon), germanium films have been studied more extensively than silicon films because they are considerably easier to fabricate. Sloope and Tiller (1963) have reviewed the work done on germanium.

Studies of silicon films have been limited to examinations of the growth and structure of the films, and to the relationship between the structure and conditions of formation of the films. Manasevit and Simpson (1964) have studied the structure of films formed on sapphire by the hydrogen reduction of $SiCl_4$. Mendelsson (1964) has reported stacking faults in silicon films formed by hydrogen reduction of $SiCl_4$ on variously oriented silicon substrates. Bicknell, Charig, and Joyce (1964) have examined films formed on single crystal quartz by hydrogen reduction of trichlorosilane. Silicon films deposited on to silicon substrates by vacuum evaporation have been examined by Handelman and Povilonis (1964), Widmer (1965), and Booker and Unvala (1964 and 1965). Silicon films vacuum deposited on to polycrystalline graphite and polycrystalline sapphire have been reported by McAleer, Pollak and Kallmann (1964) and Doo (1964) respectively, while Kataoka (1962) has investigated silicon films vacuum deposited on to fused quartz.

2. THE GROWTH AND STRUCTURE OF FILMS AND THE EFFECT OF STRUCTURE ON THE ELECTRICAL PROPERTIES OF SEMICONDUCTORS

2.1 Structure of Films

2.1.1 Film Growth

Reviews of film nucleation and growth have been presented by Pashley (1965), Hirth and Pound (1963), and Rhodin and Walton (1963). In brief, the initial growth of vacuum deposited films can be resolved into three parts: 1) the condensation of the vapour atoms on to the substrate, 2) the formation of polyatomic nuclei, and 3) the growth of the nuclei into larger aggregates.

Of the total number of silicon atoms which strike a substrate during the initial moments of bombardment, a certain fraction will immediately rebound from the surface, while the remainder become adsorbed. At sufficiently high temperature an adsorbed atom may have an appreciable probability of acquiring sufficient thermal energy to overcome the local attractive forces binding it to its immediate site. It may then move to a new position on the substrate. The surface mobility of the adatom* depends not only on the nature of the substrate lattice, but also on the smoothness of the substrate and the nature of adsorbed material on its surface. If the temperature is high enough, atoms may acquire sufficient thermal energy to leave the surface completely. If the concentration of adatoms is large enough, sufficient adatoms may come together by fluctuations to form a stable nucleus on the surface. The number of adatoms

* An adsorbed atom is referred to as an adatom.

which form a nucleus must be large enough that the decrease in free energy associated with the periodic crystalline structure of the nucleus is greater than the increase in free energy due to the surface energy of the nucleus. Once a nucleus has formed, additional adatoms join the nucleus in such a way that their free energy is a minimum. The lattice of the nucleus may have a preferred orientation relative to that of the substrate. As additional adatoms join nucleation centers at many points on the surface these nuclei grow larger and eventually overlap, forming a continuous, oriented film.

If the temperature of the substrate is high enough, atoms may re-evaporate at the same rate as they arrive at the substrate without enough adatoms accumulating on the surface to allow the formation of nuclei. Thus above a certain "critical temperature" films will not grow. It is apparent that the critical temperature is dependent upon the rate of arrival of atoms at the surface.

If the temperature of the substrate is low enough, the adatoms are immobile and the resulting film will be amorphous. In general, one expects a transition from strongly oriented to less oriented to amorphous overgrowth with decreasing temperature of deposition.

2.1.2 Overgrowth Defects

Since the lattice parameters of an oriented overgrowth are not necessarily the same as those for the substrate, there is a "misfit" at the interface. This misfit gives rise to

"interfacial dislocations" as shown schematically in Figure 1.

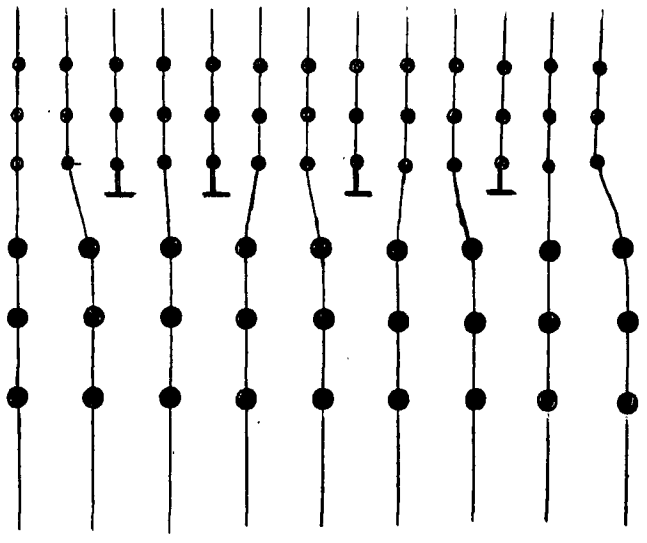

Figure 1 Schematic Representation of Interfacial Dislocations

The model in Figure 1 is according to the theory presented by van der Merwe (1963). This theory suggests that the misfit between crystals with different lattice parameters would be accomodated partly by strains in the lattices and partly by a grid of misfit dislocations. Such dislocations have been observed experimentally by Matthews (1961) (1963), and by Grübaum and Mitchell (1963).

Even when an overgrowth is deposited on a substrate of the same material (ie. silicon on silicon) defects, such as stacking faults, are present in the overgrowth. As explained by Mendelsson (1963), these stacking faults originate at defects on the substrate and extend through the overgrowth. Defects on the substrate surface such as slip lines, microscratches, dust particles, and oxide stains may result in stacking faults in the overgrowth. Such faults can be controlled by choosing an

appropriate temperature of deposition and treating the surface of the substrate suitably prior to evaporation.

2.2 Electrical Properties

In this section, the electrical properties of bulk silicon are treated first, starting with the computation of majority carrier concentration from the impurity concentration and type. Scattering mechanisms which determine the mobility of the charge carriers are then discussed. This is followed by a treatment of the modifications to the electrical properties of the bulk material by surfaces, grain boundaries, and high dislocation densities in the films.

2.2.1 Bulk Material

Charge Neutrality

During the fabrication of a single crystal bulk specimen the impurity concentration is carefully controlled. The majority carrier concentration can be calculated from the known concentration of impurities by applying the condition of charge neutrality.

Charge neutrality must hold in the interior of a bulk semiconductor. Equating the positive charges to the negative charges yields

$$p + (N_D - n_D) = n + (N_A - p_A) \qquad 2.1$$

The difference $(N_D - n_D)$ is the concentration of ionized donor sites. Similarly $(N_A - p_A)$ is the concentration of ionized acceptor sites. If more than one donor or acceptor level occurs

in the material, a sum must be taken over all such levels.

$$p + \sum_i N_{Di} - \sum_i n_{Di} = n + \sum_j N_{Aj} - \sum_j p_{Aj} \qquad 2.2$$

For a non-degenerate semiconductor (a semiconductor in which the net doping is not high enough to cause the Fermi level to lie within kT of either the conduction or valence band) the following expressions hold:

$$p = 2\left(\frac{m_p\, kT}{2\pi \hbar^2}\right)^{\frac{3}{2}} e^{-\frac{(E_F - E_V)}{kT}} = N_V\, e^{-\frac{(E_F - E_V)}{kT}} \qquad 2.3$$

and

$$n = 2\left(\frac{m_n\, kT}{2\pi \hbar^2}\right)^{\frac{3}{2}} e^{-\frac{(E_C - E_F)}{kT}} = N_C\, e^{-\frac{(E_C - E_F)}{kT}} \qquad 2.4$$

It can be show (see Spenke (1958)) that

$$n_D = \frac{N_D}{1 + \frac{1}{2} e^{\frac{E_D - E_F}{kT}}} \qquad 2.5$$

and

$$p_A = \frac{N_A}{1 + 2e^{\frac{E_F - E_A}{kT}}} \qquad 2.6$$

for particular donor and acceptor levels respectively, each with no excited states.

The charge neutrality for a typical bulk silicon specimen with N_A acceptor impurities is given in equation 2.7.

$$p = n + (N_A - P_A) \qquad 2.7$$

$$= N_c\, e^{-\frac{E_c - E_F}{kT}} + N_A - \frac{N_A}{1 + 2e^{\frac{E_A - E_F}{kT}}} \qquad 2.8$$

Solving equations 2.3 and 2.8 for p at different temperatures yields the variation of p with temperature as shown in Figure 2.

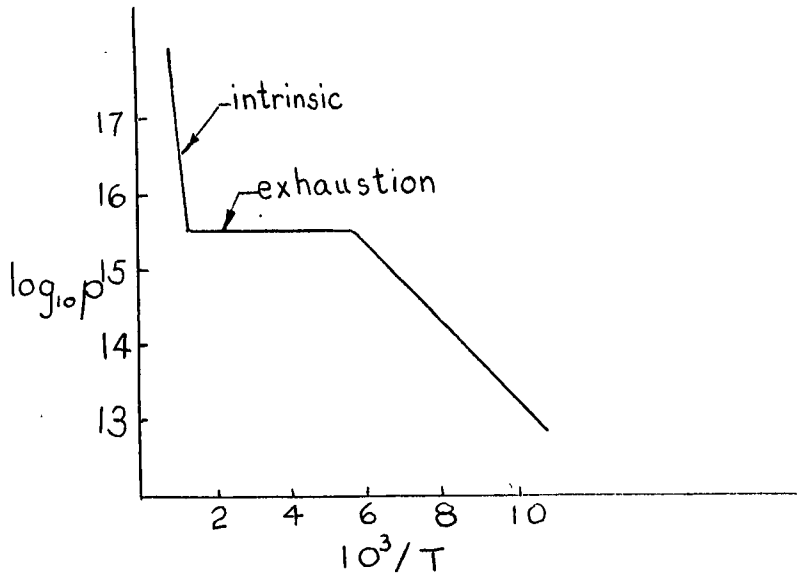

Figure 2 Variation of Hole Concentration with Temperature in a Typical Semiconductor

If many acceptor and donor levels are present in the semiconductor, compensation occurs and information relating to individual levels becomes difficult to obtain.

Scattering Mechanisms

The conductivity of a "p type" bulk specimen is given by

$$\sigma \approx pq\mu_p \qquad 2.9$$

Given the hole concentration, as determined from the impurity levels using charge neutrality, the conductivity is determined by the majority carrier mobility. The mobility of the charge carriers is, in turn, determined by the dominant scattering mechanism in the material. A free current carrier moving in a crystal lattice is scattered by departures from perfect periodicity in the lattice. A bulk crystal with few impurities, point defects, dislocations, and no grain boundaries will exhibit the highest carrier mobility. The above imperfections can be minimized by carefully controlling the production process. However, scattering by vibrating atoms in regular lattice sites (phonon scattering) cannot be eliminated.

Lattice Scattering

W. Shockley and J. Bardeen (1950a and b) have derived an expression for the dependence of mobility on temperature for acoustic lattice scattering as shown in equation 2.10.

$$\mu = \frac{2^{3/2}\,\pi^{\frac{1}{2}}\,q\hbar^4 du_l^2}{3m_p^{5/2}\,E_l^2(kT)^{3/2}} \qquad \text{(esu)} \qquad 2.10$$

where E_l is a constant independent of temperature. This expression is not entirely accurate, as indicated by Morin and Maita (1954); however, it does give approximately the right variation of mobility with temperature.

Uncharged Impurity Scattering

The effect of scattering by neutral impurities has been discussed by J. Bardeen and G.L. Pearson (1949), who

arrived at the expression

$$\mu_u = \frac{q}{20 a_1 \hbar N_n} \qquad \text{(esu)} \qquad 2.11$$

N_n = concentration of neutral impurities

$a_1 = (\frac{m}{m'})(\frac{\varepsilon}{\varepsilon_o})\, a_o$

where a_o = radius of Bohr orbit

$= \frac{\hbar^2}{m}$

This expression states that μ_u is independent of temperature.

Charged Impurity Scattering -- Non-degenerate

Conwell and Weisskopf (1946) have derived the following expression which describes carrier mobility as a function of temperature and impurity concentration when the dominant scattering mechanism is by ionized impurities.

$$\mu_{IN} = \frac{2^{3/2}\, K^2\, (2kT)^{3/2}}{\pi^{3/2}\, N_I\, Z^2\, q^3\, m^{\frac{1}{2}}} \left[\ln \left\{ 1 + \left(\frac{3K\, kT}{Z^2\, N_I^{1/3}} \right)^2 \right\} \right]^{-1} \qquad \text{(esu)} \qquad 2.12$$

Equation 2.12 is applicable to non-degenerate semiconductors only.

Charged Impurity Scattering -- Degenerate

Ionized impurity scattering under conditions of degenerate doping has been discussed by Johnson and Lark-Horowitz (1947a and b). The theory they presented is an extension of the theory of Conwell and Weisskopf (1946) presented in the above section. Mobility of charge carriers under

conditions of degeneracy is given by equation 2.13.

$$\mu_{ID} = \left(\frac{4q}{h}\right)\left(\frac{3}{\pi}\right)^{-1/3} p^{2/3} \quad \text{(esu)} \qquad 2.13$$

Degeneracy is the result of a hole concentration being large enough to cause the Fermi level to lie within kT of the valence band. Therefore, virtually all acceptors are ionized and the resulting hole concentration is independent of temperature. The mobility associated with a degenerately doped specimen is also independent of temperature as indicated by equation 2.13.

Scattering by Dislocations

Scattering by dislocations has been discussed theoretically by D.L. Dexter and F. Seitz (1952) and by W.T. Read (1954 and 1955). In each treatment scattering is insignificant unless there are greater than 10^8 dislocation per cm^2.

A dislocation is shown schematically in Figure 3.

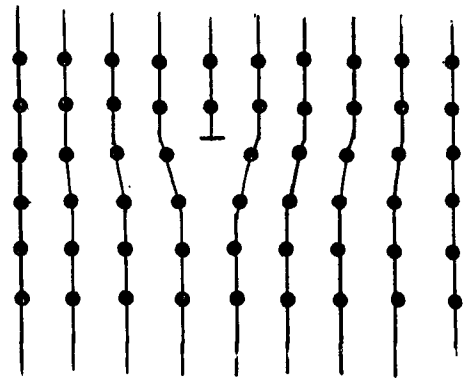

Figure 3 Representation of a Dislocation

Each atom along the line of the dislocation has a free or "dangling" bond. Each dangling bond may act as an acceptor to one electron. However, when such a bond has an addditional

electron, neighbouring bonds are likely not to accept an electron because of electrostatic repulsion. Along the dislocation, therefore, only atoms spaced sufficiently far apart can act as acceptors. The uncharged atomic sites on the dislocation will act as scattering centers, but their effect will be much less than that of the charged centers. Adjacent charged centers along a dislocation line, of necessity, have little electrostatic interaction. Hence, each such center will act as an independent point scattering source as stated previously.

Carrier Concentration and Mobility

The quantities measured experimentally are the Hall coefficient and the conductivity. The basic equations required for the calculation of the mobility and carrier concentration from measurements of the conductivity and Hall coefficient of a homogeneous semiconductor are as follows (Smith (1964), Shockley (1950), and Putley (1960)):

1) Impurity Range

p type material	n type material	
$p = \frac{\alpha}{qA_H}$	$n = \frac{-\alpha}{qA_H}$	
$\mu_H = \frac{A_H \sigma}{\alpha}$	$\mu_H = \frac{A_H \sigma}{\alpha}$	2.14
$= pq\mu_p$	$= nq\mu_n$	

2) Intrinsic Range

$$= pq\mu_p + nq\mu_n$$

$$A_H = \frac{\alpha}{q} \frac{n\gamma^2 - p}{(n\gamma + p)^2} \qquad 2.15$$

$$\text{if } n = p$$

$$= nq(\mu_p + \mu_n)$$

$$A_H = \frac{-\alpha}{nq} \frac{(\gamma - 1)}{(\gamma + 1)}$$

The numerical factor α depends upon the band structure and the predominant scattering mechanism but is seldom very different from unity. For simplicity it is assumed that $\alpha = 1$ in this study.

2.2.2 Thin Films

The macroscopic Hall coefficient and conductivity are considerably more difficult to interpret for thin films than for bulk material. The surface of the film may provide donor and acceptor states; as well, it causes additional scattering. More important, the inhomogeneity presented by the grain boundaries (which are present in the film but not usually in the bulk) can affect both the macroscopic conductivity and the Hall coefficient of the thin film. These effects are considered in more detail in the next three sections.

Surface States

As indicated in section 2.2.1, charge neutrality holds only in the interior of a semiconductor. At a surface, the dangling bonds which would otherwise be bonded to the next lattice plane can act as acceptor or donor sites. Similarly, oxides and contaminants adsorbed on the surface can provide sites which may attract or repel charge carriers. These two effects may cause an excess or deficiency of electrons close

to the surface. An accumulation of charge results in bending of the energy bands as shown in Figure 4. The space charge

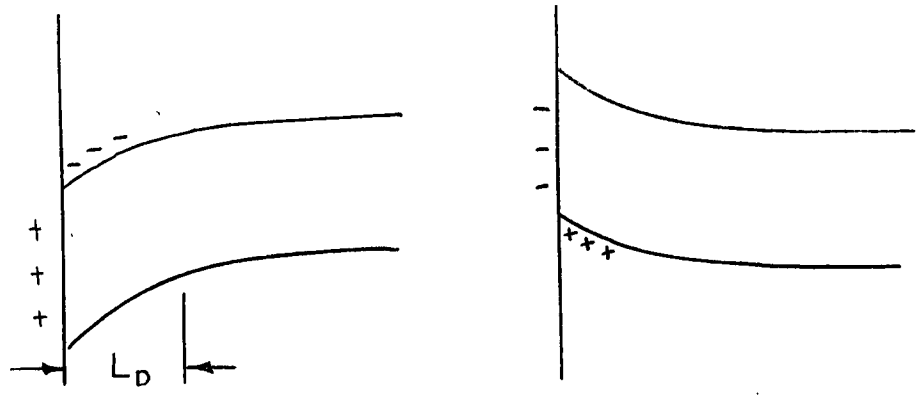

Figure 4 Effect of Surface States on the Energy Bands

region extends a distance of the order of a Debye length (L_D) from the surface of the semiconductor. The Debye length is given in equation 2.16.

$$L_D = \sqrt{\frac{KkT}{4\pi q^2 p}} \quad \text{(esu)} \qquad 2.16$$

For silicon with $p = 10^{14}$ holes/cm^3, the Debye length is approximately 5×10^{-5} cm at room temperature.

Surface Scattering

Reduction of mobility occurs whenever the carriers are confined to move in a region whose width is comparable to the mean free path of the carriers (ie. in a very thin film). The amount of scattering of the carriers by surface atoms depends on the roughness of the surface. If the surface is perfectly smooth, scattering is specular, but if the surface is

rough, scattering is diffuse to some extent*. The relative amounts of diffuse and specular scattering are difficult to predict and must be determined experimentally. Since the thinnest film studied (0.35μ) is much thicker than the mean free length of carriers in bulk silicon ($\sim$0.002μ), surface scattering is expected to be negligible. (See Many, Goldstein and Grover (1965) and Ziman (1963) for reviews of surface scattering.)

The Polycrystalline Film Model

Any interpretation of the electrical properties of a polycrystalline material must take into account the effect of inhomogeneities due to grain boundaries. The actual disorder at the grain boundaries probably extends only a few lattice parameters (at most 100A°). The defects in the grain boundaries however have electronic states associated with them which may cause the energy bands to bend at the boundaries (similar to the band bending caused by surface states). The effect of bands bending at the grain boundaries extends approximately one Debye length into each adjoining crystallite. For a film in which the crystallites are more p type than the grain boundaries, the energy bands will bend at these boundaries as shown in Figure 5.

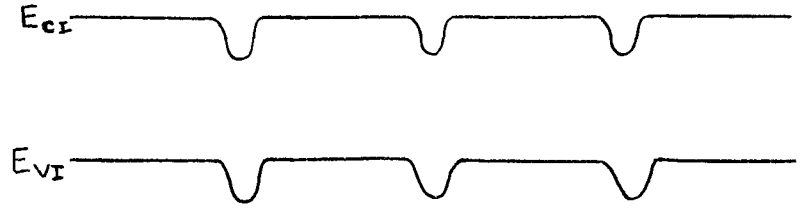

Figure 5 Band Bending Caused by Grain Boundaries

* Specular scattering is scattering in which the magnitude of the momentum of the carrier is unchanged upon collision; the sign of the component of momentum perpendicular to the scattering surface changes. Diffuse scattering is scattering in which the momentum of the carrier after collision is random.

Volger (1950) has proposed a model similar to that shown in Figure 6 to treat a polycrystalline film. The squares (regions I) represent crystallites which are separated by grain boundaries (region II). Regions I and II are assumed to differ in resistivity and hole concentration. It is assumed that the film is one crystallite thick, and that there is no variation in resistivity in the Z direction.

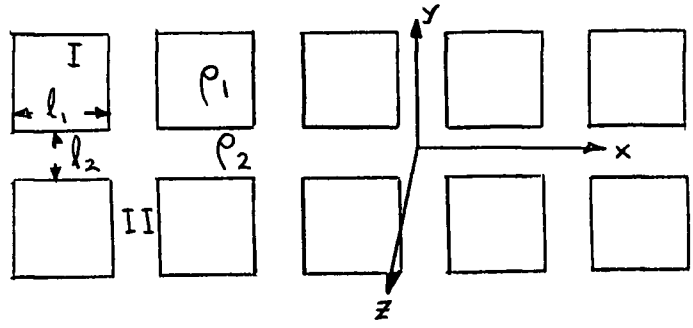

Figure 6 The Inhomogeneous Film Model

Volger has stated that the macroscopic resistivity of this model is approximately

$$\bar{\rho} \simeq \rho_1 + \rho_2 \, l_2/l_1 \qquad 2.17$$

and that the Hall coefficient is approximately

$$\bar{A}_H \simeq A_{H1} + k\left(\frac{l_2}{l_1}\right)^2 A_{H2} \qquad \text{(where } k \simeq 1\text{)} \qquad 2.18$$

if it is assumed that $l_1 \gg l_2$ and $\rho_1 \ll \rho_2$.

Volger dealt only with the case in which the grain boundary regions have a much higher resistivity than the crystallite regions. Since it is conceivable that the grain boundaries may have a lower resistivity than the crystallites, a more general case is now treated.

The model in Figure 6 is approximately equivalent (insofar as conductivity is concerned) to the network shown in Figure 7. No resistors are included between nodes of adjacent rows of resistors in Figure 7 because these points are

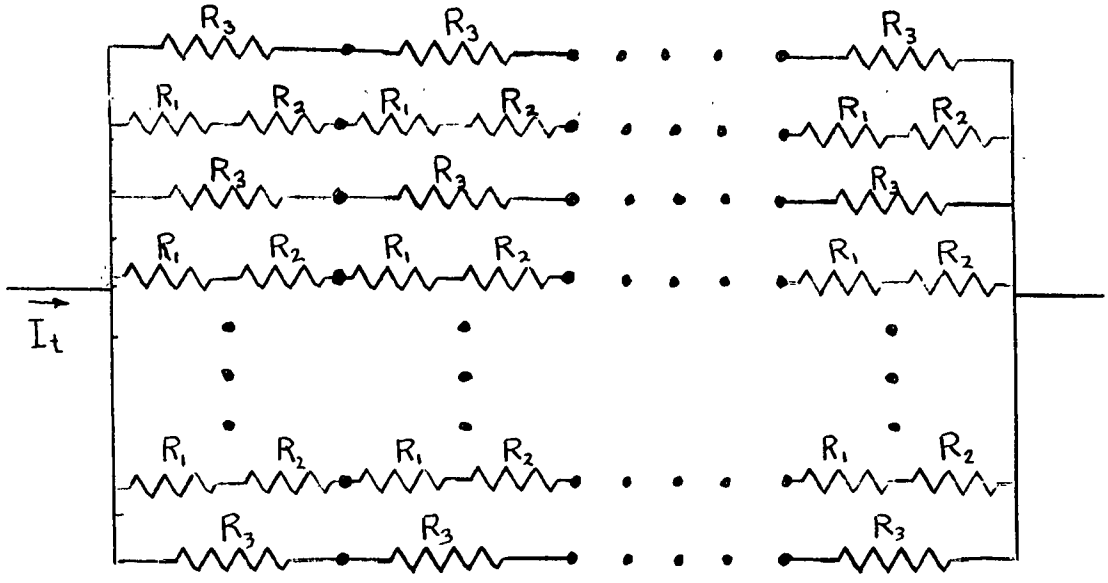

Figure 7 Resistive Analog of Inhomogeneous Film Model

at equal potentials. In this network

$$R_3 = \rho_2 \frac{l_1 + l_2}{l_2 t} , \qquad 2.19$$

where t is the thickness of the film,

$$R_1 = \rho_1 / t, \qquad 2.20$$

and

$$R_2 = \rho_2 l_2 / l_1 t. \qquad 2.21$$

The total resistance of the network is

$$\bar{R} = \frac{N}{n} \frac{R_3(R_1 + R_2)}{R_1 + R_2 + R_3} , \qquad 2.22$$

where N is the number of crystallites in the length of the specimen and n is the number of crystallites in the width of the specimen. In terms of the macroscopic resistivity of the specimen ($\bar{\rho}$)

$$\bar{R} = \frac{N}{n} \frac{\bar{\rho}}{t} \qquad 2.23$$

Substituting equations 2.19, 2.20, 2.21, and 2.22 into 2.23 yields

$$\bar{\rho} = \frac{\rho_2(l_1 + l_2)(\rho_1 + \rho_2 \frac{l_2}{l_1})}{l_2\left[\rho_1 + \rho_2(1 + \frac{l_1}{l_2} + \frac{l_2}{l_1})\right]} \qquad 2.24$$

The Hall coefficient ($\bar{A}_H$) of the inhomogeneous film model of Figure 6 is defined by

$$\bar{A}_H = \frac{\bar{V}_H\, t}{I_t\, B} \qquad \text{(mks)} \qquad 2.25$$

where $\bar{V}_H$ is the Hall voltage

and I_t is the total current passing through the film. The Hall voltage may be regarded as being generated by the combination of Hall voltages from the different regions of the inhomogeneous film model as shown in Figure 8.

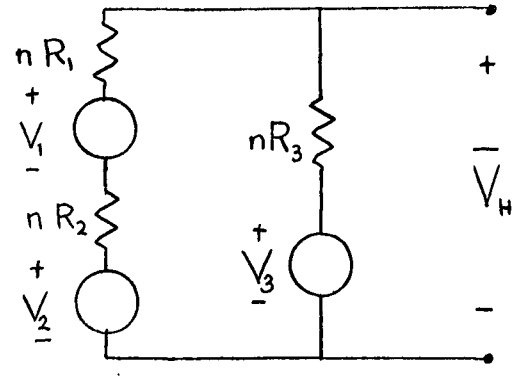

Figure 8 Hall Voltage Analogue of Inhomogeneous Film Model

where

$$V_1 = A_{H1}\, I_1\, B/t, \qquad 2.26$$

$$V_2 = A_{H2}\, I_2\, B/t, \qquad 2.27$$

$$V_3 = (A_{H2}\, I_2 + cA_{H2}\, I_1)\, B/t, \qquad 2.28$$

$$I_1 = R_3 I_t/(R_1 + R_2 + R_3), \qquad 2.29$$

and $$I_2 = (R_1 + R_2) I_t/(R_1 + R_2 + R_3). \qquad 2.30$$

The coefficient c in equation 2.28 is caused by the tendency of the current contacts to "short" the Hall voltage in short, wide specimens (Putley (1960) p. 45). In this model, the Hall voltage of the grain boundaries which are perpendicular to the length of the specimen is shorted appreciably only if $\rho_1 < \rho_2$. If $\rho_1 \geq \rho_2$, then the crystallites do not short the Hall voltage of the grain boundaries appreciably and $c \simeq 1$. If $\rho_1 \ll \rho_2$, c is a function of l_1/l_2 as shown in Figure 9.

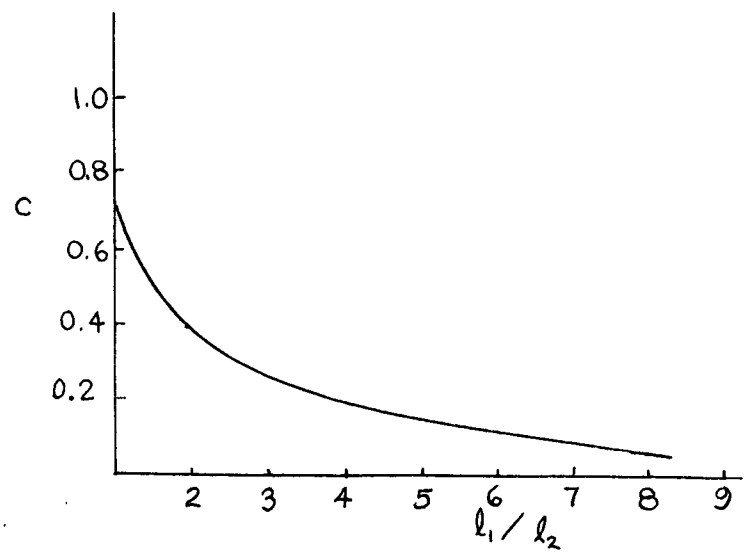

Figure 9 Shorting Effect of Contacts on the Hall Coefficient

If $\rho_2 \ll \rho_1$ the grain boundaries will tend to short the Hall voltage generated by the crystallites. The crystallites are assumed to be square. As shown in Figure 9, the factor which corrects for shorting in a square specimen is $\simeq 0.70$. The accuracy of results obtained by representing the actual film with the model in Figure 6 and then by representing this model by networks of discrete components is expected to be approximately 50%. For this reason the factor of 0.70 associated with the shorting of square specimens is taken as unity.

The open circuit voltage of the network in Figure 8 is given by

$$\bar{V}_H = \frac{R_3(V_1 + V_2) + (R_1 + R_2)V_3}{R_1 + R_2 + R_3} \qquad 2.31$$

Substituting equations 2.19, 2.20, 2.21, 2.26, 2.27, 2.28, 2.29, 2.30, and 2.31 into equation 2.25 yields

$$\bar{A}_H = \frac{A_{H1}\left[\rho_2\left(\frac{l_1+l_2}{l_2}\right)\right]^2 + A_{H2}\left(\rho_1+\rho_2\frac{l_2}{l_1}\right)\left(\rho_2\left(\frac{l_1+l_2}{l_2}\right)(1+\alpha)+\rho_1+\rho_2\frac{l_2}{l_1}\right)}{\left[\rho_1 + \rho_2\left(1+\frac{l_1}{l_2}+\frac{l_2}{l_1}\right)\right]^2} \qquad 2.32$$

Equations 2.24 and 2.32 reduce to equation 2.17 and 2.18 respectively when $l_1 \gg l_2$ and $\rho_1 \ll \rho_2 \frac{l_2}{l_1}$.

3. EXPERIMENTAL PROCEDURE AND APPARATUS

In this chapter a description of the evaporation apparatus and the preparation of the specimens is given. This is followed by a description of the Hall effect testing apparatus and measurement techniques. Finally a brief account of the interpretation of electron diffraction patterns is presented.

3.1 Preparation of Films

3.1.1 Description of the Vacuum System

The silicon films were produced by evaporating a block of silicon in vacuum, and allowing the silicon vapour to deposit on substrates in the system. The source block of silicon and the substrates were housed in a stainless steel shell which was mounted on a ten inch diffusion pump (NRC #H.S.10 - 4200). A Meissner cold trap was included in the upper portion of the shell as well as the conventional nitrogen cold trap between the interior of the shell and the diffusion pump. The system gave a vacuum of 3×10^{-8} torr after pumping overnight with no refrigerant in the trap and then pumping with liquid nitrogen in the trap for 30 minutes. During an evaporation it was capable of maintaining a vacuum in the range of 5×10^{-7} to 1×10^{-6} torr.

The source and the substrate were heated by bombardment with an electron beam. The target block of silicon was held in a copper cold hearth through which water was passed to

prevent the copper from melting.

Five substrates were mounted in the system, with only one substrate being exposed to the molten silicon target at a time. Hence, five specimens could be made without breaking the vacuum. To heat each substrate as uniformly as possible an electron beam was scanned over the back of the substrate in a Lissajous figure. Each substrate was backed with platinum and tantalum to prevent negative charge from building up on the insulating substrate, thus deflecting the electron beam. The back of each substrate was held at ground potential through tantalum support clasps.

A photograph of the evaporation unit and one electron gun power supply is shown in Figure 10.

3.1.2 Preparation of Substrate and Source

Prior to each set of evaporations, the source block of silicon was chemically polished in CP4 (5 parts by volume of 70% HNO_3, 3 parts 55% HF, 3 parts glacial Acetic acid). The source was outgassed while in place in the cold hearth by heating until molten with an electron beam.

The substrates (except CaF_2 which is soluble) were cleaned in hot trichloroethylene vapour, bathed in acetone, and finally rinsed in distilled water. (The CaF_2 substrate was used as produced by the supplier.) Each substrate was outgassed, prior to deposition, for five minutes at 1100°C. Aside from cleaning, the substrates were used as received from the suppliers. (The Al_2O_3 was obtained from Adolph Meller & Co. and the CaF_2 and MgO were obtained from Semi-Elements Inc.) All substrates

as received had been mechanically polished and showed few microscratches under optical examination.

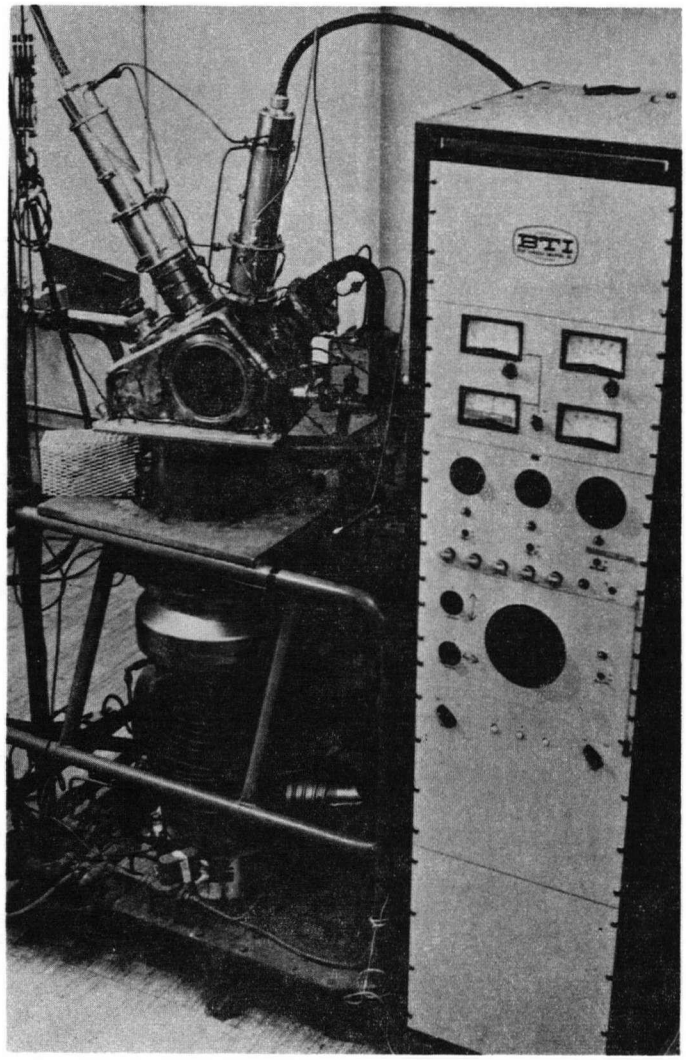

Figure 10 The Evaporation System

3.1.3 Evaporation Procedure

Prior to later evaporations the interior of the shell was outgassed for several hours by heating to red heat a nichrome heating coil inside the shell. The shell was then allowed to cool before a fabrication run began. During an

evaporation, contamination from adsorbed material on the interior walls of the shell was minimized by cooling the exterior of the shell with cold water which was circulated through copper pipes attached to the outside of the shell. At ten minute intervals during an evaporation, the temperature of the substrate was measured with an optical pyrometer*. The pyrometer was calibrated with an iron-constantan thermocouple by Salama (1966). The pressure was recorded at ten minute intervals during an evaporation run. The entire run was timed. In some runs the thickness of film deposited was monitored using a Sloan Deposit Thickness Monitor, Model DTM2a. The frequency of oscillation of the monitor, which was proportional to the thickness of film deposited, was read when the system was cold before the film was deposited and again when the system was cold after the deposition. The thickness of the grown film was also measured using the infra-red interference technique described by Albert and Combs (1962) and Salama (1966).

3.2 Electrical Measurements

To be able to measure the specimens in this study, the measurement apparatus had to be capable of measuring low carrier mobilities (1 cm^2/v-sec.) of high resistance specimens ($10^{10}\Omega$). The low mobilities gave rise to Hall voltages as small as one millivolt. Thus, the measurement apparatus had to be sensitive to these small Hall voltages. The high resistance made measurement by a.c. methods impractical since the RC constant of the

---

* Pyropto, Hartmann and Braun, Frankfurt/Main, Germany.

circuit could be as large as five seconds. Therefore, a d.c. supply voltage was used. Noise pick-up associated with high resistances was also an important factor to be considered in design of the circuit.

3.2.1 Description of Circuit

The Hall effect measuring apparatus is shown in Figure 11.

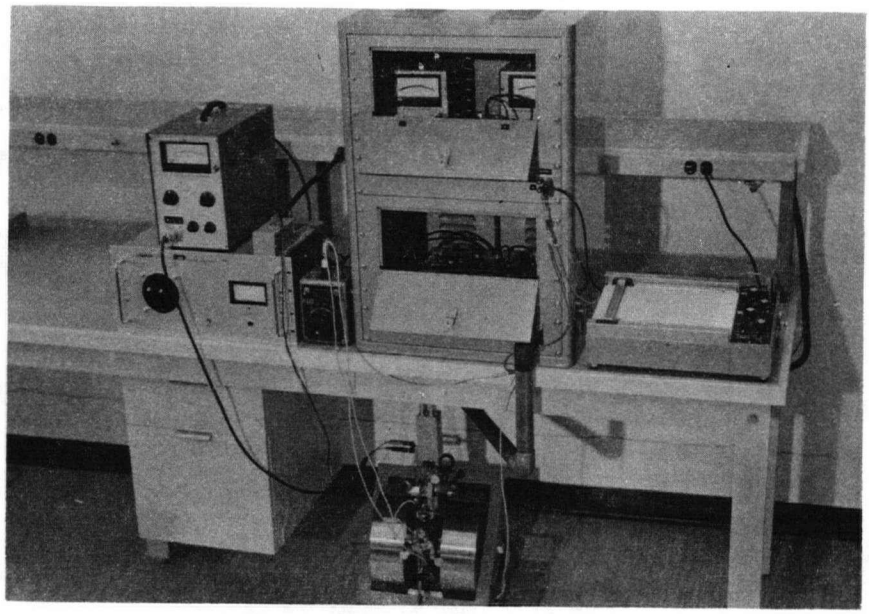

Figure 11 The Hall Effect Apparatus

The circuit of this apparatus is shown in Figure 12.

Specimens with resistances up to 10^{10} ohms could be measured conveniently with this apparatus. Specimens of greater resistance could not be measured accurately since the time constant of the circuit became comparable to the time constant associated with drift of the measuring circuit.

Keithley 600-A electrometers with input impedences of 10^{14} ohms were employed to avoid loading the circuit during

measurement of the voltages on the side-arms of the specimen.

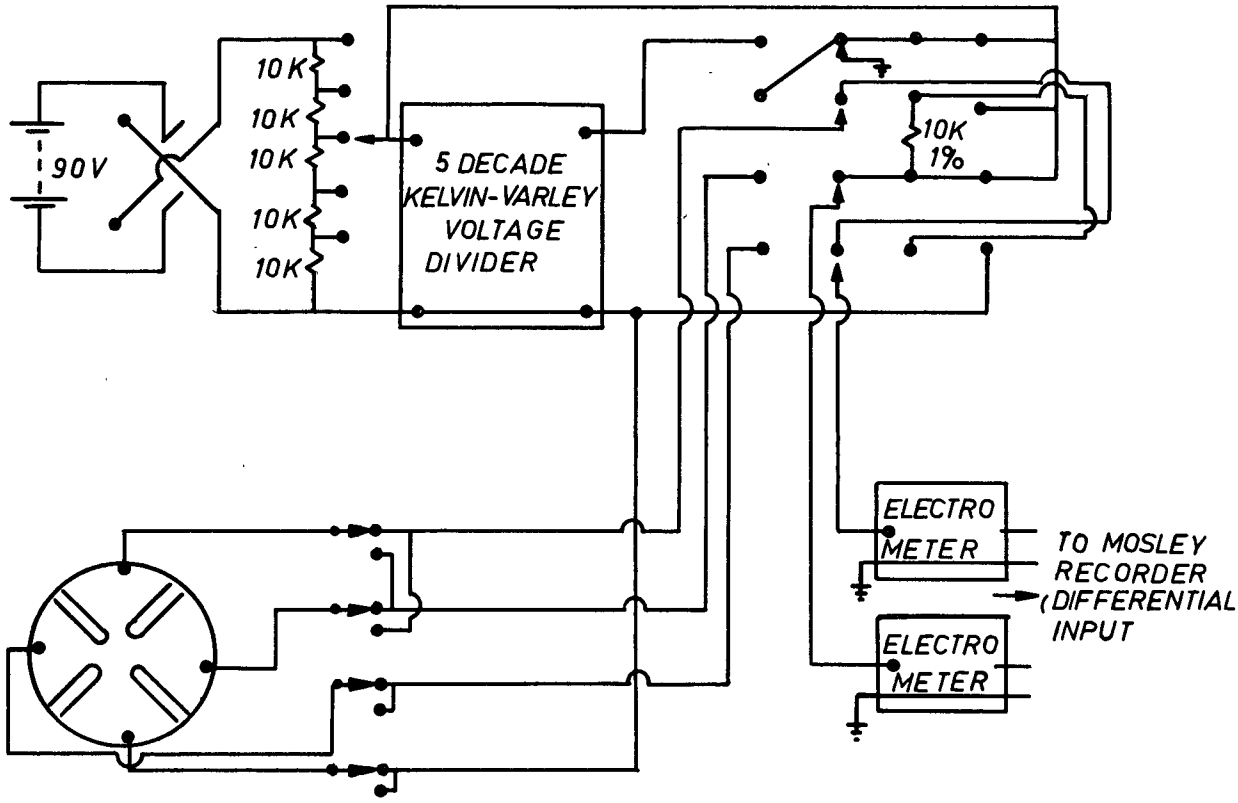

Figure 12 Circuit of Hall Effect Apparatus

In order that leakage paths to ground were negligible (greater than $10^{+13}\Omega$) teflon insulated lead wires were used. The specimen holder was also composed of teflon (see Figure 13).

Double shielding was employed in all portions of the circuit which were susceptible to noise pick-up.

Common mode suppression was employed to eliminate noise pick-up in parallel leads (ie. the leads were wrapped together so that noise picked up in one lead was also picked up

in the other; therefore the difference in signals on the two leads was unaffected by common noise).

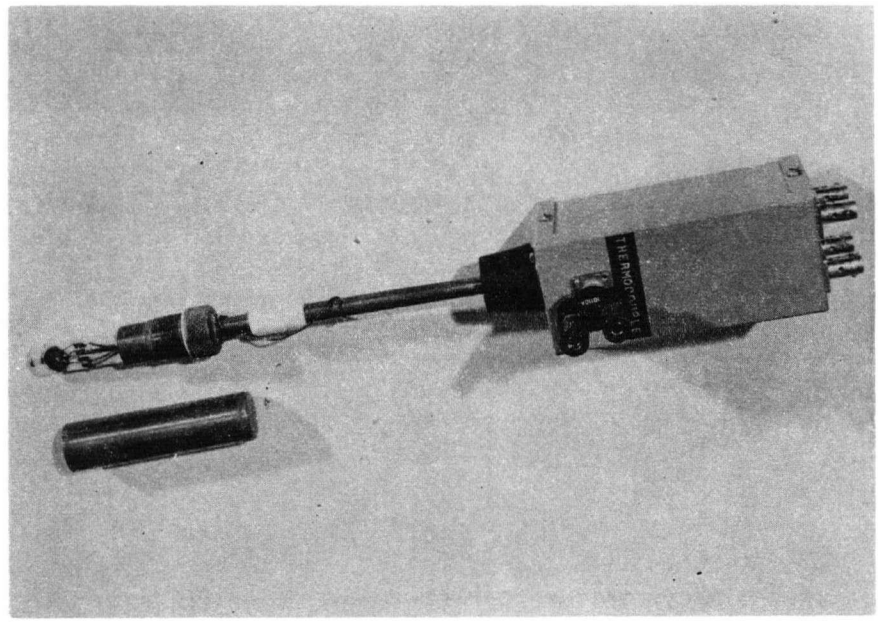

Figure 13 The Specimen Holder

The Hall voltage was measured as the difference between the outputs of the two electrometers. The d.c. voltage resulting from the offset of the Hall probes on the specimen was cancelled with a potentiometer on the output of one electrometer. The Hall voltage was recorded on a Moseley X-Y (model 135) recorder for fifteen to twenty seconds to obtain an average value.

The magnetic field (generated by an Alpha P8500 power supply and Alpha 8500 magnet) was measured with a Hall probe Gaussmeter (RFL model 1890). A field of 6 Kilogauss was used to provide as large a Hall voltage as possible without causing high field effects.

3.2.2 Accuracy of Measurements

Accuracy in measuring the conductivity was governed by the accuracy of the Keithley electrometers. In the ranges used the electrometers were accurate to $\pm$ 3%. Measurement of temperature was accurate to $\pm$ 4°C.

The greatest inaccuracy was encountered in measuring the Hall voltage. In the case of very thin films ($\sim$ 0.3μ) the peak to peak noise superimposed on the Hall voltage was comparable to the magnitude of the Hall voltage. The resulting accuracy of measurements was estimated at 50%.

The gradual warming of the specimens at low temperatures ($<$240°K) caused a drift in the offset voltage. This drift caused some difficulty in determining the Hall voltage of the high resistance specimens because the rate of drift was comparable to the response time of the circuit (which was long because of the large R.C. constant associated with high resistance specimens at low temperatures). The accuracy of measurements under these conditions is estimated to be approximately 50%. Inaccuracy due to noise and drift for specimens greater than 0.3 microns thick and at temperatures greater than 240°K was estimated at less than 15%.

Thermoelectric and thermomagnetic effects were calculated to be negligible.

3.2.3 Specimen Holder and Heating/Cooling System

The specimen holder is shown in Figure 13. The specimen was heated in an electric furnace which was held in

place between the pole pieces of the magnet. Cooling was achieved by immersing the specimen and specimen holder in liquid nitrogen. The cold specimen and specimen holder were put into an insulating jacket of polystyrene foam between the pole pieces of the magnet and measurements were taken while the specimen warmed to room temperature. The thermal time constant of the specimen in its insulating jacket was approximately one half hour. The maximum change of temperature during the time required to take one set of measurements (approximately one minute) was found to be less than $0.5^{o}C$.

The temperature of the specimen was measured with an iron-constantan thermocouple. The thermocouple was imbedded in a copper disc upon which the back of the substrate rested when the substrate was in place in the specimen holder. Good thermal contact between the copper disc and the substrate was ensured by applying a drop of glycerin to provide high thermal conductivity between the disc and the substrate.

3.2.4 The Specimen

The technique of measuring conductivity and Hall coefficient discussed by van der Pauw (1958) was used in this study. This technique was convenient because only the thickness of the film had to be known (see Appendix I).

Contacts

As explained by van der Pauw, the error in measurement due to non-infinitesimal contacts is minimized by using the

"four leaf clover" configuration shown in Figure 14. For the "four leaf clover" configuration H. J. van Daal (1965) has shown that less than 3% error is introduced in conductivity measurements when the diameters of the contacts are one quarter the diameter of the specimen.

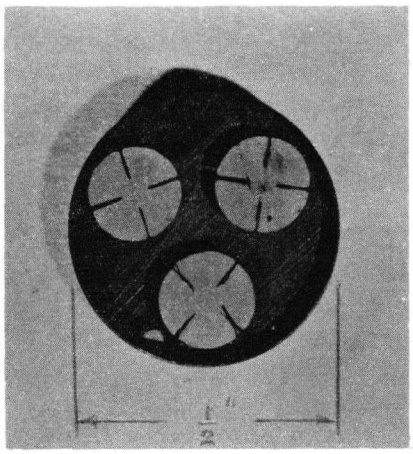

Figure 14 A Substrate Showing Three Specimens

Ohmic contacts to the films were made successfully by the following two methods:

a) Aluminum was evaporated through a mask onto the silicon film. The aluminum was then alloyed into the silicon by heating the specimen to approximately 600°C in a vacuum of 10^{-6} torr. A pressure contact was then made to the aluminum.

b) A portion of the oxide was scratched from the silicon film using a sharp point. Indium was subsequently soldered onto the scratched area using a fine point soldering iron. A contact wire was then soldered onto the indium.

Both methods yielded low noise ohmic contacts. Since the latter contact was easier to make, it was used most extensively.

Photoetching of Specimens

Each film was photoetched into three specimens as shown in Figure 14. The photoetching procedure was as follows:

1) The film was covered with a coating of KMER (Kodak Metal Etch Resist) approximately one to two microns thick. The KMER was then dried for twenty minutes under infra-red lights.

2) The portion of the specimen which was to be etched away was covered with a suitable photographic mask.

3) The specimen thus masked was exposed for three minutes to ultra-violet light from a Foto Foil vacuum printer*. The ultra-violet light polymerized the exposed portion of the resist, yielding it insoluble to most normal acids and solvents.

4) The specimen was then bathed in KMER developer for three minutes to remove the unexposed resist and to assist in toughening the polymerized resist.

5) The specimen was then bathed for several seconds in CP4 until all undesired silicon film was removed from the substrate.

6) The remaining resist was removed by bathing in KMER developer for several minutes and wiping with a clean cloth.

Inhomogeneities

Three specimens were etched on each substrate to provide a check for uniformity of film properties at different points on the substrate. Any differences in electrical properties would be caused largely by uneven heating of the substrate during deposition.

---

* Miller Dial and Nameplate Co.

Macroscopic inhomogeneities in the film were also indicated by the variation of the ratio $R_{AB,CD}/R_{BC,DA}$ (Appendix I) with temperature. For a homogeneous sample the ratio $R_{AB,CD}/R_{BC,DA}$ should be a constant, only determined by the geometry of the sample.

3.3 Electron Diffraction

The structure of the films was investigated by electron diffraction. The films were too thin for study by X-ray diffraction. No method was found of detaching the silicon films from the sapphire for examination by transmission electron microscopy, therefore glancing angle diffraction was used to examine the films. An Hitachi 11A electron microscope was used.

The electron diffraction pattern (Pinsker (1953), Thompson and Cochrane (1939)) of single crystal material is an array of single dots. The position of the dots depends on the geometry of the electron diffraction apparatus, the type of crystal lattice, and the orientation of the lattice with respect to the incident electron beam. Diffraction by a polycrystalline powder produces a diffraction pattern which is composed of concentric rings. Such rings are the result of diffraction from lattice planes in many possible orientations.

A diffraction pattern which has both dots and circles present is caused by a polycrystalline material which has some "preferred orientation". Completely disoriented or amorphous material yields diffuse rings on the photographic plate.

The degree of crystallinity of the silicon films in

this study has a marked effect on the electrical properties of the films. Therefore, the electron diffraction patterns are used primarily as an indication of crystallinity. The problem of relative orientations of silicon overgrowths on sapphire substrate, has been examined by Manasevit and Simpson (1964).

4. FILM GROWTH AND STRUCTURE

In this chapter the growth and structure of films prepared on 0° and 60° sapphire is discussed*.

4.1 Effect of Rate of Arrival of Vapour Atoms on Growth of Initial Grains

Figures 15 a to 15d show the nucleation of silicon on 0° sapphire. Each film was grown for one hour at $950^{\circ}C$. The rate of arrival of silicon atoms was increased for each specimen shown in each successive photomicrograph in Figure 15.

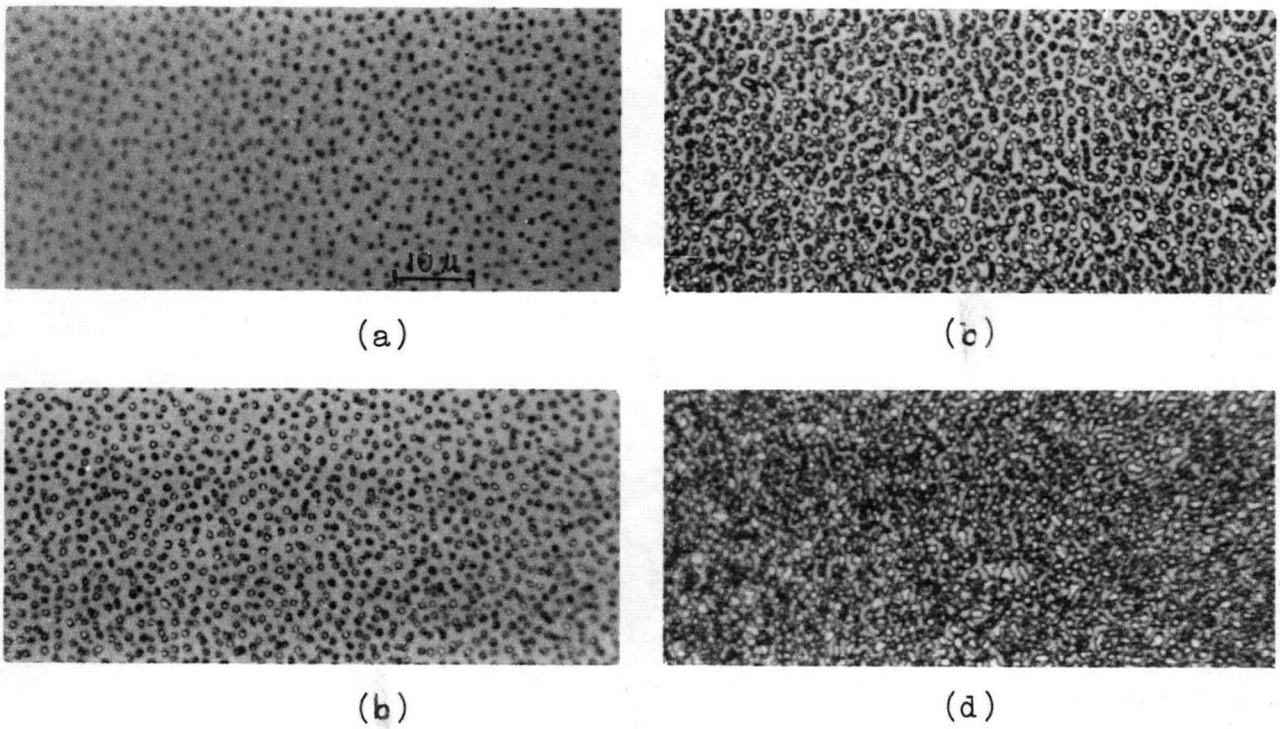

Figure 15 Photomicrograph of the Growth of Initial Grains (at $950^{\circ}C$ on 0° Sapphire)

---

* 0° sapphire is the conventional term for sapphire which has the normal to the surface plane of the sapphire inclined at 0° to the $\langle 0001 \rangle$ axis of the sapphire. 60° sapphire has the normal to the surface inclined at approximately 60° to the $\langle 0001 \rangle$ direction; this is the direction of fast growth of the sapphire crystal.

The first nuclei grown (which were observable optically) are shown in Figure 15a. With an increased rate of arrival of silicon atoms the nuclei were larger and more plentiful (Figure 15b). The nuclei began to overlap and form chains of nuclei width a still larger rate of impinging atoms (Figures 15c and 15d). (Growth of silicon films on quartz by the formation of chains of nuclei has been observed by Bicknell et al (1964).)

4.2 Growth of Film after Becoming Continuous

Figure 16 shows the first continuous layer of film deposited at 950°C. As additional layers were grown on top of this first layer, the crystallites became larger and indicated a higher degree of orientation (as indicated by the diffraction patterns in Figure 17).

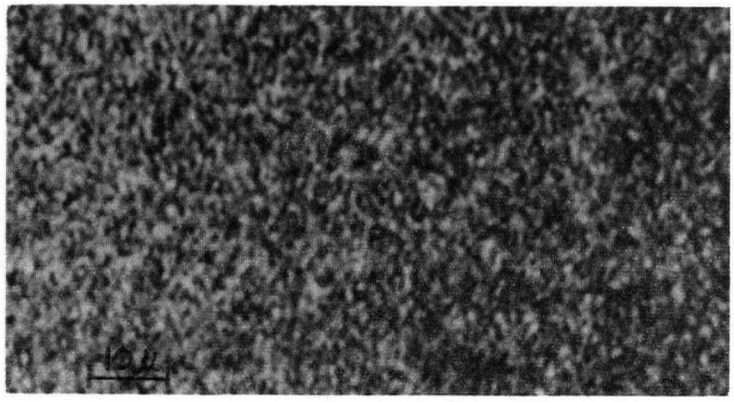

Figure 16 Photomicrograph of Film 0.1μ Thick Deposited at 950°C onto 60° Sapphire

The film shown in Figure 16 was about 0.1μ thick; the film shown in Figure 19(b) was also grown at 950°C and was about 0.6μ thick. It is evident that the crystallites are larger for the thicker film.

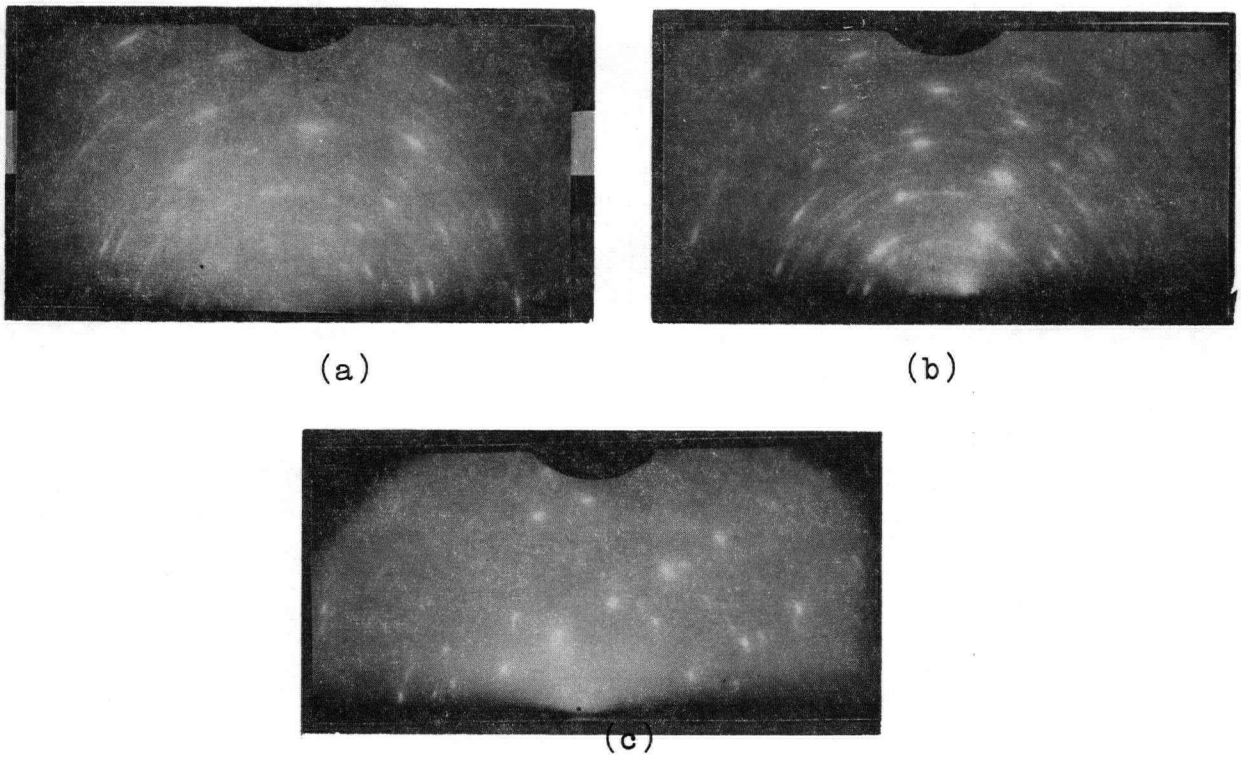

Figure 17 Diffraction Patterns of Films of Various Thickness Deposited at 950°C onto 60° Sapphire

4.3 Effect of Microscratches on the Substrate

Figure 18 shows a film grown at 1060°C. At this temperature the concentration of adatoms is small and the nuclei are unstable. Hence, nucleation occurs most readily at defects (such as microscratches on the substrate surface).

Figure 18 Photomicrograph of a Film Grown at 1060°C on 0° Sapphire Showing Preferred Nucleation at Microscratches

Several rows of nuclei which have formed on microscratches on the substrate are evident in Figure 18.

4.4 Variation of Crystallite Dimensions with Substrate Temperature and Orientation

Figure 19 shows photomicrographs of films grown at 850°C, 950°C, and 1050°C on 0° sapphire. It shows that the average size of the crystallites increased with temperature of deposition until the critical temperature was approached. Within a few degrees of the critical temperature the size of the crystallites decreased very rapidly.

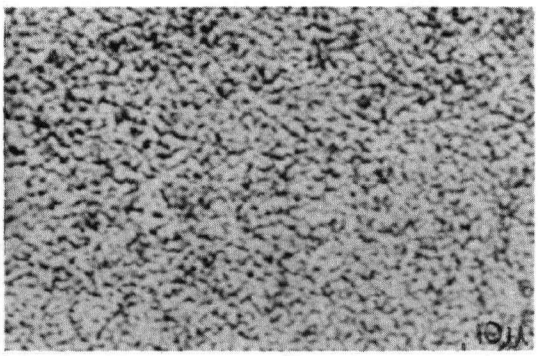

850°C
(a)

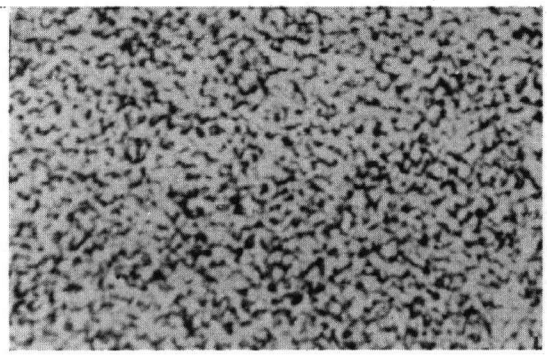

950°C
(b)

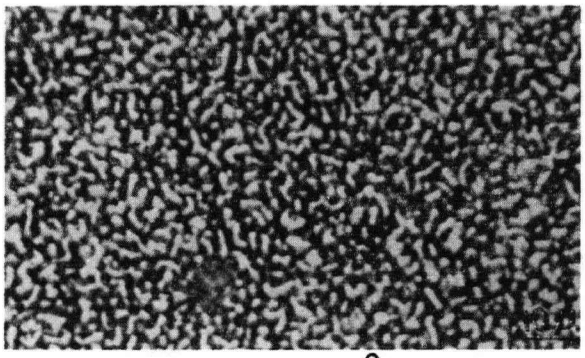

1050°C
(c)

Figure 19 Photomicrographs of Films Deposited on 0° Sapphire at Various Temperatures

Figure 20 shows the variation with deposition temperature of the average length of the crystallites in the final continuous film (as estimated from photomicrographs) of films grown on 0° and 60° sapphire.

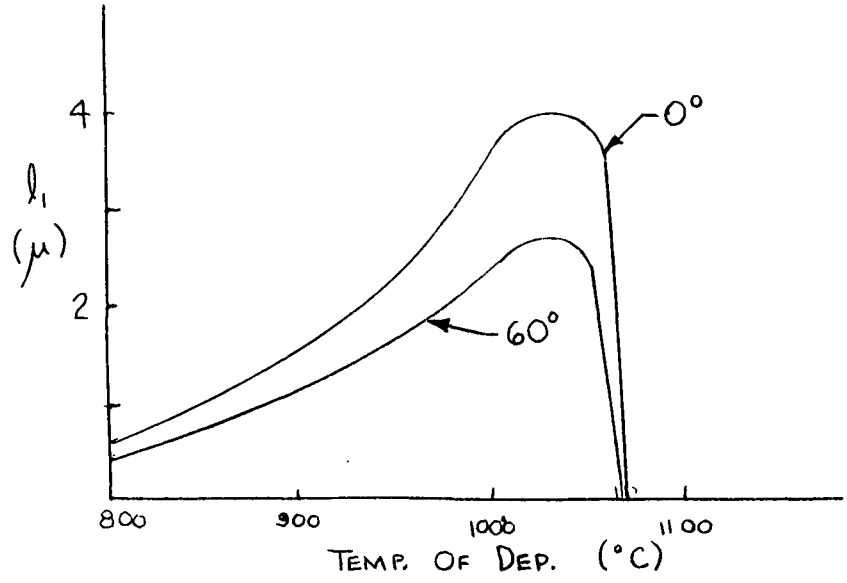

Figure 20 Variation of Average Crystallite Size with Temperature of Deposition

The electron diffraction pattern in Figure 21 shows the effect of temperature of deposition on overgrowth orientation. There is a greater degree of orientation apparent as the deposition temperature is increased.

4.5 Effect of Lattice Orientation in the Substrate

The orientation of the substrate lattice may be expected to have an effect on the orientation of crystallites in the overgrowth. This is verified by Figure 22, which shows specimens deposited at the same temperatures as those in Figure 21. However, the films whose diffraction patterns are

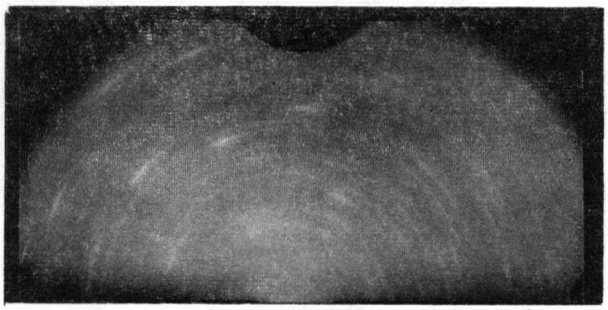

(a)
#17 850°C

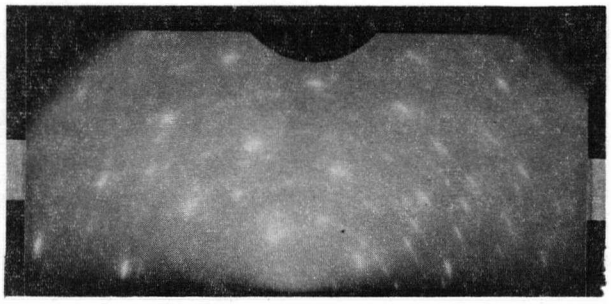

(b)
#15 950°C

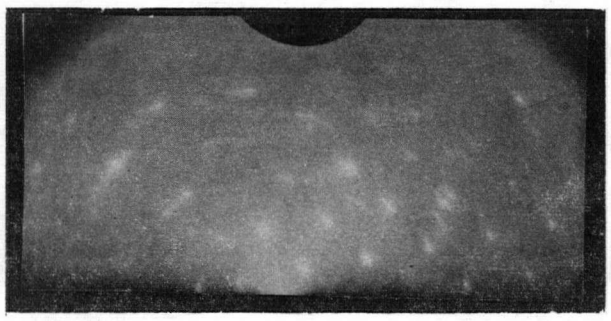

(c)
#14 1050°C

Figure 21
Electron Diffraction Patterns
of Films Deposited on 60°
Sapphire at Various Temperatures

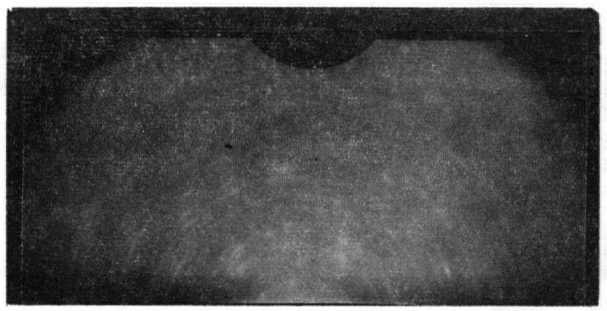

(a)
#10 850°C

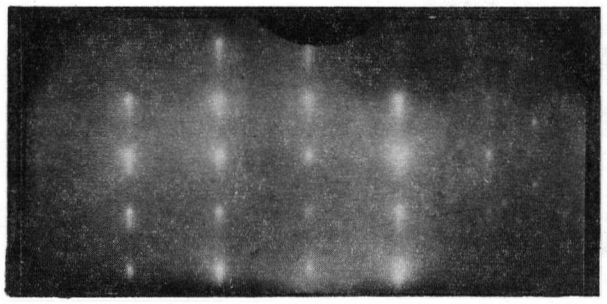

(b)
#25 950°C

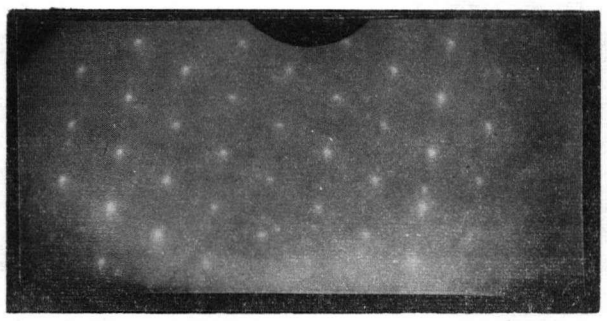

(c)
#11 1050°C

Figure 22
Electron Diffraction Patterns
of Films Deposited on 0°
Sapphire at Various Temperatures

shown in Figure 22 were grown on 0° sapphire. It is evident that films grown on 0° oriented sapphire are more oriented than those grown on 60° sapphire.

4.6 Variation of the Rate of Film Growth with Substrate Temperature

Figure 23 shows the variation of film growth rate with substrate temperature, for a particular concentration of impinging silicon atoms. The concentration of the beam of silicon atoms striking the substrate depended on the power input to the silicon target by electron bombardment, the power withdrawn by cooling from the cold hearth, and the distance from the molten target to the substrate. For each specimen shown in Figure 23 the distance from source to substrate, the rate of cooling, and the bombarding energy were kept the same.

Up to $1040^{\circ}C$ the film thickness (ie. the average growth rate) decreased approximately linearly with increasing temperature. Above $1040^{\circ}C$ the rate of growth decreased very rapidly and at approximately $1070^{\circ}C$, no silicon deposited. This rapid decrease in growth rate is a result of the small number of nucleation centers formed as the critical temperature is approached.

4.7 Summary

The growth of silicon films occurs by the formation of nuclei which then grow together to form a continuous film. This mechanism is consistent with the discussion in Chapter 2 of this thesis. Crystallites grew progressively larger and

more oriented with increasing film thickness. In addition, the crystallites became larger and more oriented with increasing temperature of deposition. Within a few degrees of the critical temperature, nucleation was observed to occur more readily on microscratches on the substrate than on smooth portions of the substrate. The crystallites grown on 0^{o} sapphire were larger and more oriented than crystallites grown on 60^{o} sapphire.

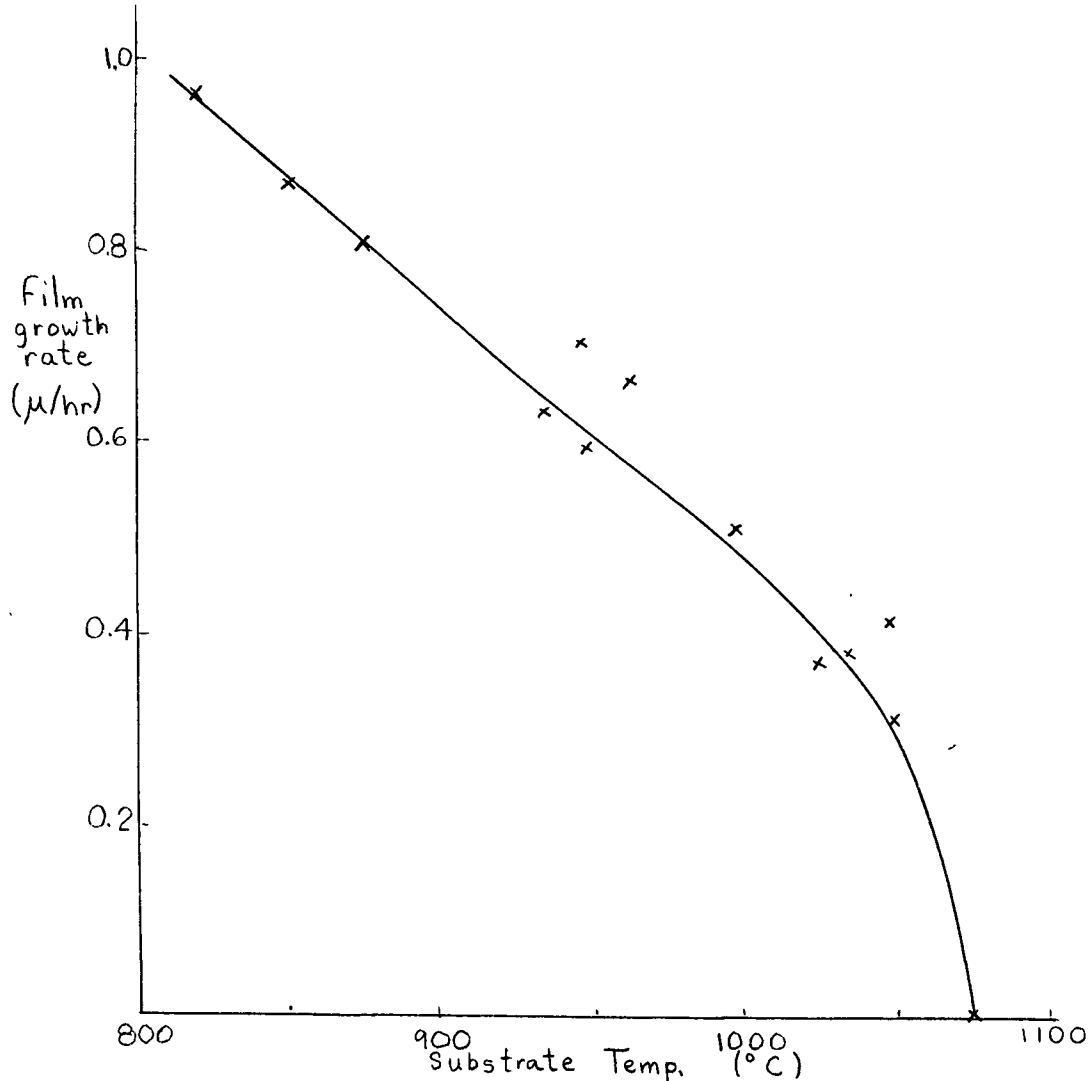

Figure 23 Variation of Average Growth Rate of Film with Temperature of Deposition

5. ELECTRICAL PROPERTIES

In this chapter the electrical properties of films deposited under various conditions are presented. The dependence of the properties of the films on thickness is discussed first. A general discussion of typical features of the electrical properties is then presented. This is followed by a discussion of the effect of dopant of the source (n or p) on the electrical properties of the films. The effect of orientation of the lattice of the substrate (0° and 60° sapphire) is examined next. Finally, a discussion of reproducibility and homogeneity of the films is presented.

5.1 Effect of Film Thickness

Films of thicknesses 0.35μ, 0.62μ, and 1.7μ were deposited on 60° sapphire at 950°C. The films 0.62μ and 1.7μ thick exhibited less than a factor of 2 difference in resistivity, effective hole concentration* and Hall mobility (as shown in Figures 24, 25, and 26). The hole concentration of the 0.35μ film was less by a factor of 10 than that of the thicker films, suggesting that the bands were bent down at one or both surfaces. Since the extent of the effect of band-bending at a surface is one Debye length, it was concluded that the thickness of the 0.35μ film was comparable to a Debye length. In the remainder of the study the films used were approximately 0.6μ thick and it is a reasonable approximation to neglect surface states.

---

* Effective hole concentration is defined by $\bar{p} = \frac{1}{A_H q}$

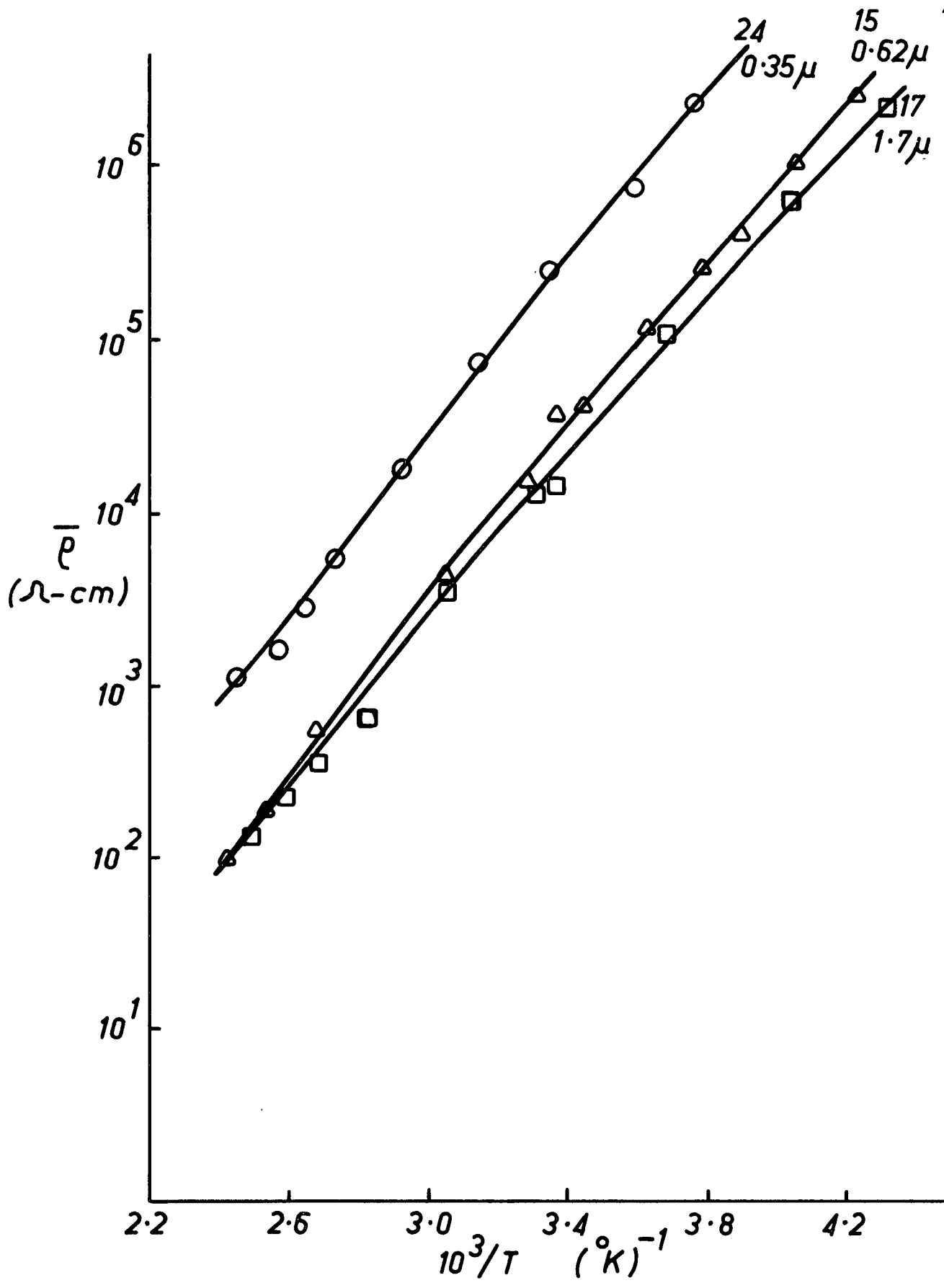

Figure 24 Resistivity vs. Temperature for Films of Various Thicknesses Deposited at 950°C on to 60° Sapphire from a p type Source

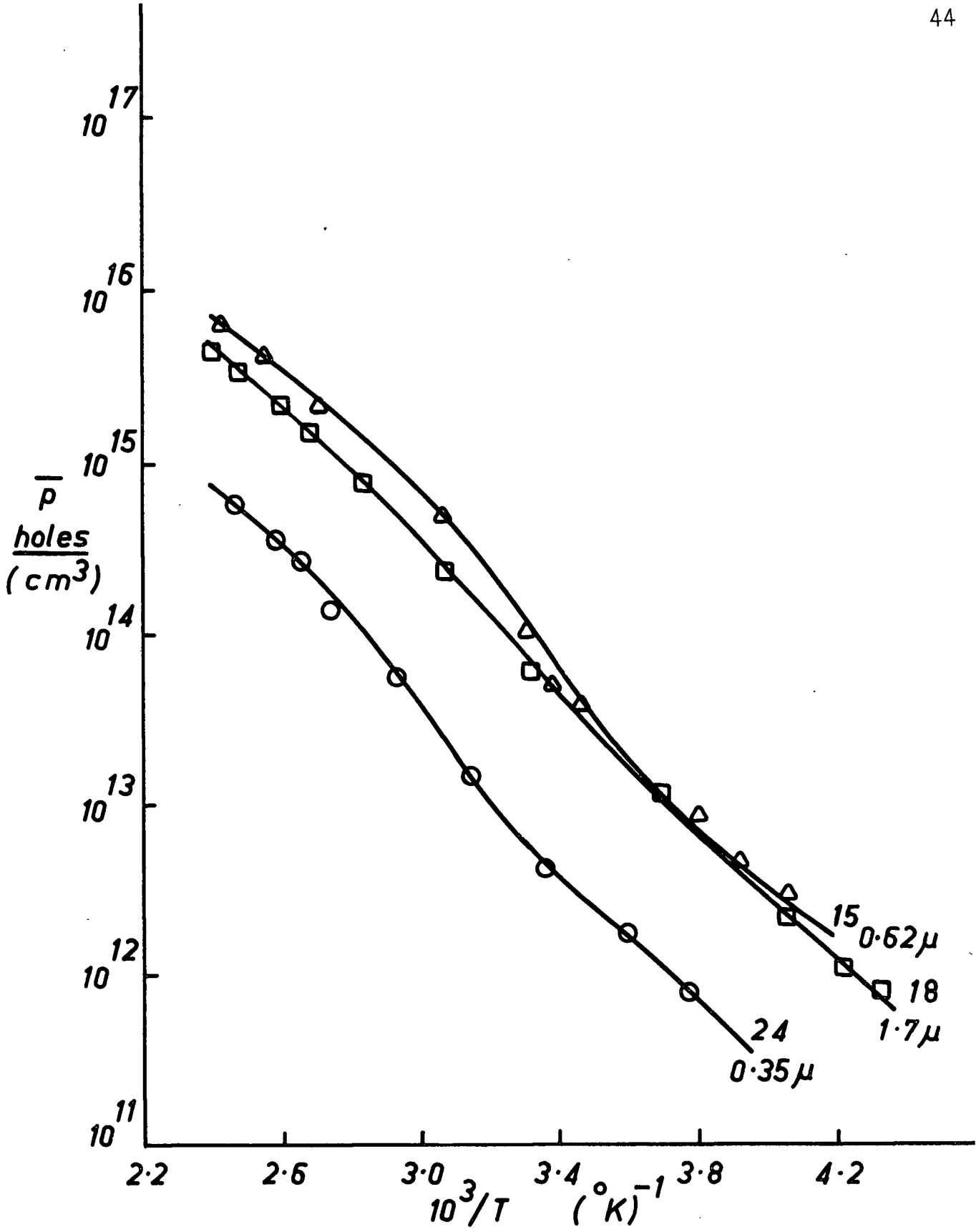

Figure 25 Hole Concentration vs. Temperature for Films of Various Thicknesses Deposited at 950°C on to 60° Sapphire from a p type Source

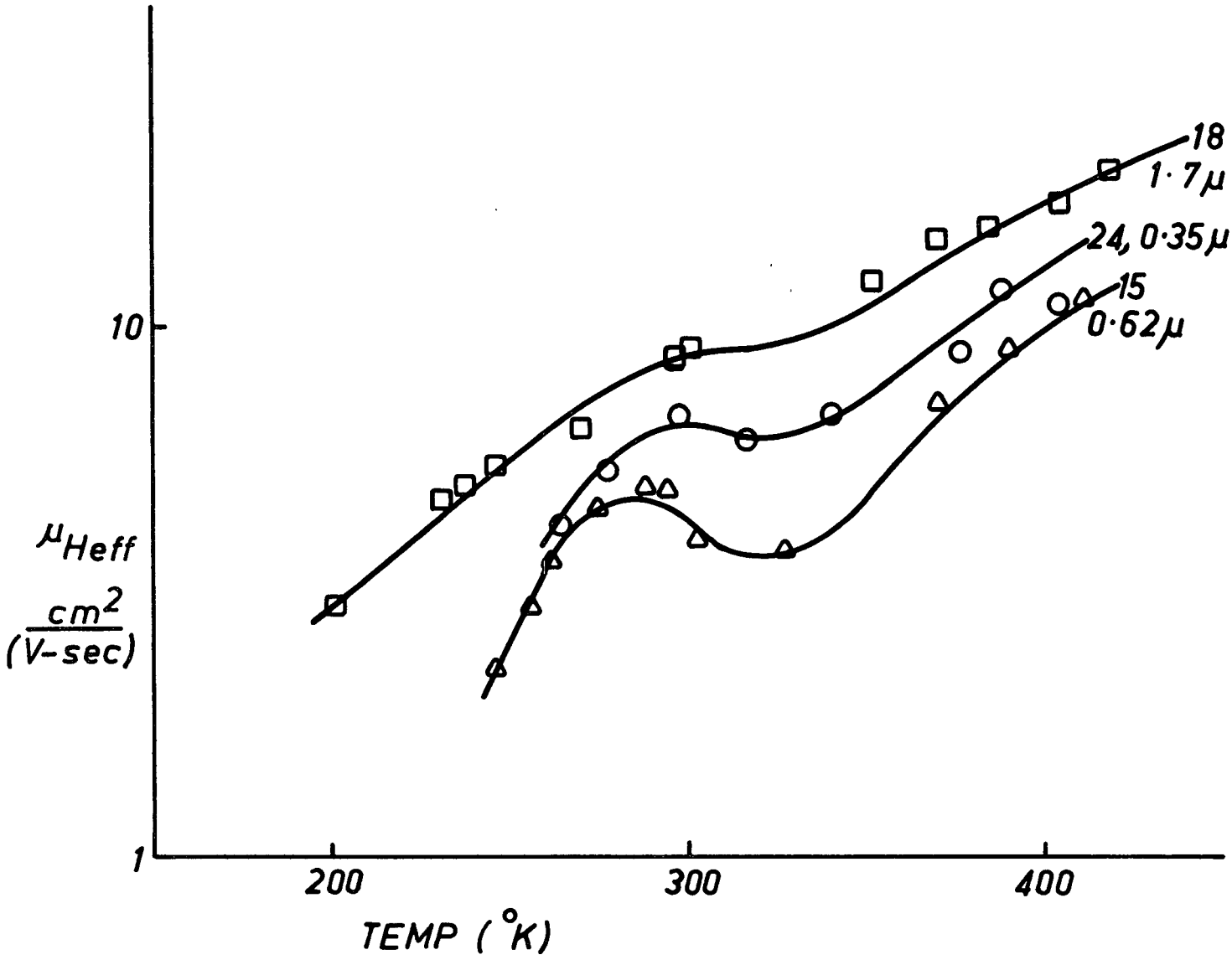

Figure 26 Hall Mobility vs. Temperature for Films of Various Thicknesses Deposited at 950°C on to 60° Sapphire from a p type Source

5.2 General Discussion

All specimens had a positive Hall coefficient at room temperature. The effective hole concentrations of most films deposited at 950°C or less were similar to those shown in Figure 25, in that they a) displayed a steady decrease in effective hole concentration with decreasing temperature and b) had a very low hole concentration, as low as commercially available high purity bulk material at the same temperature. The Hall coefficient from which the effective hole concentration was calculated is determined in terms of the properties of the grain boundaries and crystallites by equation 2.32. By using simplifying assumptions, the Hall coefficient of most films studied can be related by a simple factor to the hole concentration in either the crystallites or in the grain boundaries.

A very low hole concentration is associated with either a very pure material or with both acceptor and donor levels being present in the material in such a way that they compensate one another. Since the films in this study are not of high purity the low hole concentration must be the result of heavy compensation of donor and acceptor levels. The hole concentration of silicon which has been subjected to neutron or high energy electron radiation is characteristic of heavily compensated material (Crawford and Clelland (1957) and Vavilov (1964)). The defects introduced during irradiation have associated with them both acceptor and donor levels and hence cause this compensation. Similar levels caused by defects in the silicon films must exist in the regions of the films which govern the Hall

coefficient. In order that the films be p type the acceptor levels must dominate the donor levels.

The IBM 7040 digital computer was programmed to solve the charge neutrality equation for the hole concentration at various temperatures. This was done to determine the relative effects of defect and dopant levels on the hole concentration in the discordered silicon. Acceptor levels at 0.36 ev. and 0.42 ev. and a donor level at 0.81 ev. were assumed to represent the levels introduced by defects. An acceptor level at 0.05 ev. with a concentration of 5×10^{15} acceptors/cm^3 was assumed to represent the dopant from the source. The defect level concentrations were taken to be $N_A(0.36) = N_A(0.42) = 2N_D(0.81)$ where the values $N_A = 10^{20}$, 10^{19}, 10^{18}, 10^{17}, and 10^{16} were used to find the effect of the degree of compensation. The results obtained are shown in Figure 27. For the data with a much larger defect concentration than dopant concentration the results are similar to those obtained experimentally for the films with high defect concentrations. The dopant had appreciable effect on the hole concentration only when the dopant concentration was of the same order of magnitude as the defect concentration.

Since the p type source had approximately 7×10^{17} holes/cm^3, it is postulated that greater than this number of donor and acceptor sites/cm^3 existed in the films deposited from this source at 850°C. Greater than 7×10^{17} holes/cm^3 are postulated to explain the negligible effect of the dopant from the source. It is assumed that the dopant evaporates and deposits at the same rate that the silicon does.

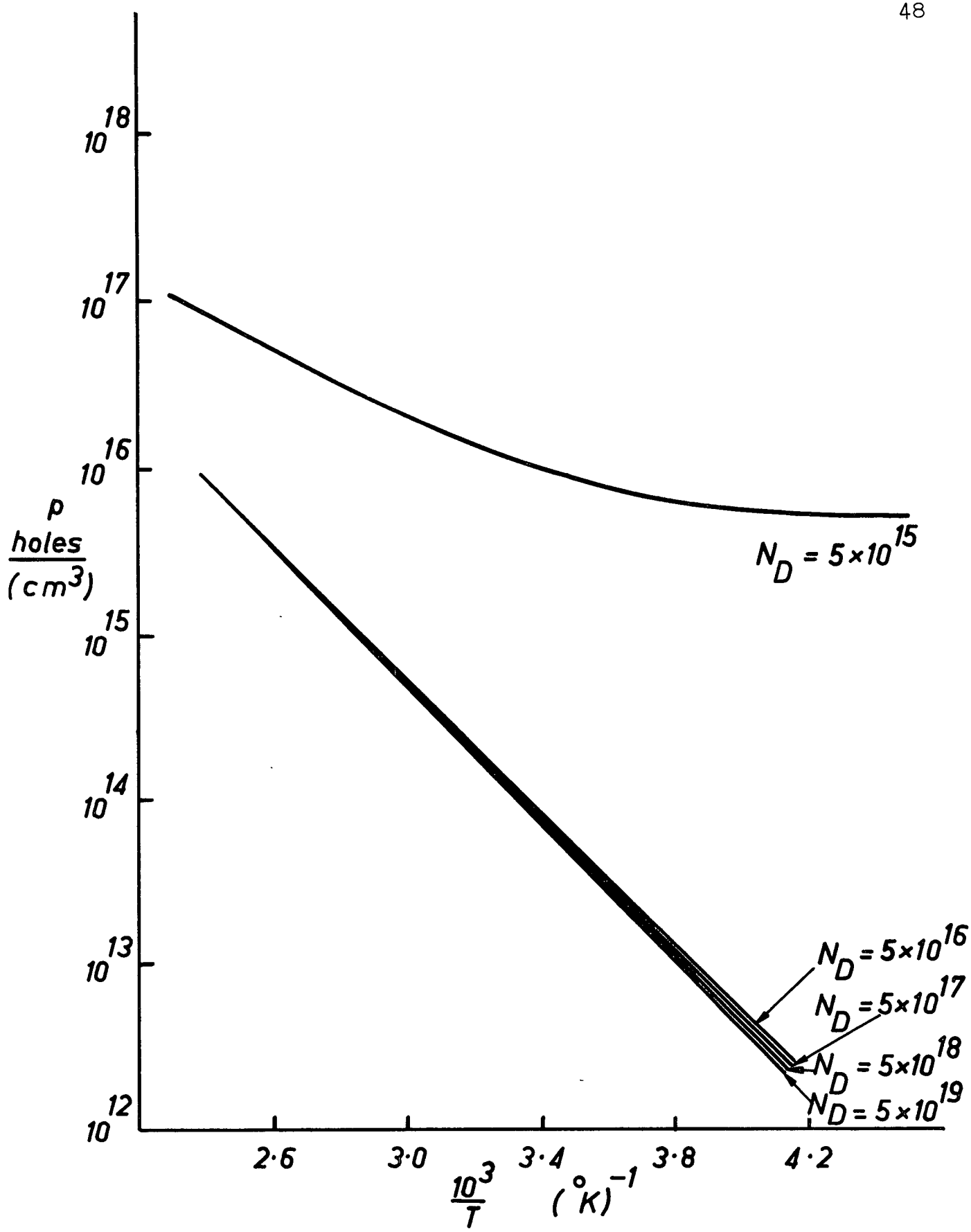

Figure 27 Hole Concentration vs. Temperature Showing Effect of the Degree of Compensation

It is expected that the grain boundaries will have a higher concentration of defects than the crystallites for all films studied. There is less compensation associated with the lower concentration in the crystallites. Therefore, it is expected that the dopant from the source will have a greater effect on the hole concentration in the crystallites than on that in the grain boundaries. Hence, at room temperature $p_1 < p_2$ when the film is made from an n type source and $p_1 > p_2$ when a p type source ss used. The two limiting cases $\rho_1 \gg \rho_2$ and $\rho_2 \gg \rho_1$ are now considered. In the first case the total resistance of the film is governed by the resistance of the grain boundaries which run the length of the specimen. (The resistance of the crystallites is assumed to be infinite compared to the resistance of the grain boundaries.) Therefore, the resistivity of the film is

$$\bar{\rho} = \rho_2 \frac{l_1 + l_2}{l_2} \qquad 5.1$$

In practice $\rho_1 \gg \rho_2$ only if an n type source is used and there are few defects in the crystallites. In the second case (which occurs when a p type source is used and there are few defects in the crystallites) the crystallites are short circuits compared to the grain boundaries. The total resistance of the film, therefore, is governed by the resistance of the boundaries which run across the specimen and is described by

$$\bar{\rho} = \rho_2 \frac{l_2}{l_1} \qquad 5.2$$

These expression can also be derived from equation 2.24 by assuming that $\rho_1 \gg \rho_2 \frac{l_1}{l_2}$ and $\rho_1 \ll \rho_2 \frac{l_2}{l_1}$ respectively. It

is interesting to note that the resistivity of the film in both cases was determined by the resistivity of the grain boundaries.

The Hall mobility which is defined by $\mu_{Heff} = \bar{A}_H \bar{\sigma}$, is the product of two terms, one of which may be determined by the grain boundaries while the other may be determined solely by the crystallite regions. Hence the Hall mobility is not related by a simple factor to the carrier mobility in either one region or the other.

Because there are three properties for each of almost a dozen specimens, a detailed discussion of each property of each specimen would be unpalatable to the reader. Therefore, only specimens from which a general trend of properties can be obtained are discussed in detail.

5.3 Effect of Temperature of Deposition

The electron diffraction results given in section 4.4 show that as the temperature of deposition was increased, the crystallites in the films were larger and had fewer defects. With fewer defects, the dopant from the source would be expected to have a greater effect on the hole concentration of the crystallites. By depositing films from 0.094 Ω-cm p type and 1 Ω-cm n type sources on to substrates at different temperatures, the relative effects of dopant and defects on the hole concentration of the film were examined.

Figure 28 shows that the resistivities of the films deposited on 0° sapphire at $850^\circ C$ from n and p type sources were not appreciably different (specimens 22 and 10 respectively).

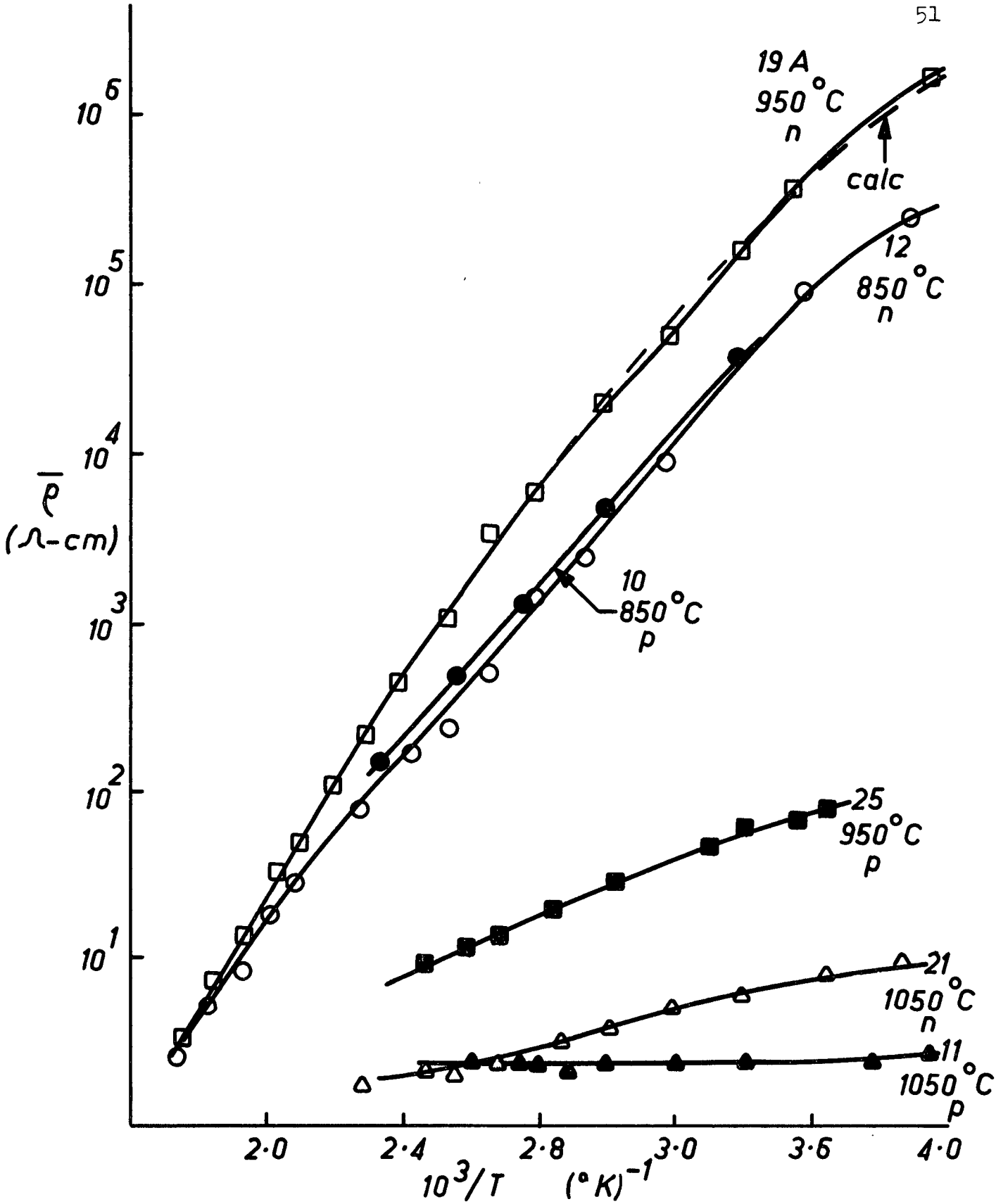

Figure 28 Resistivity vs. Temperature for Films Deposited on to 0° Sapphire at Various Temperatures from n and p type Sources

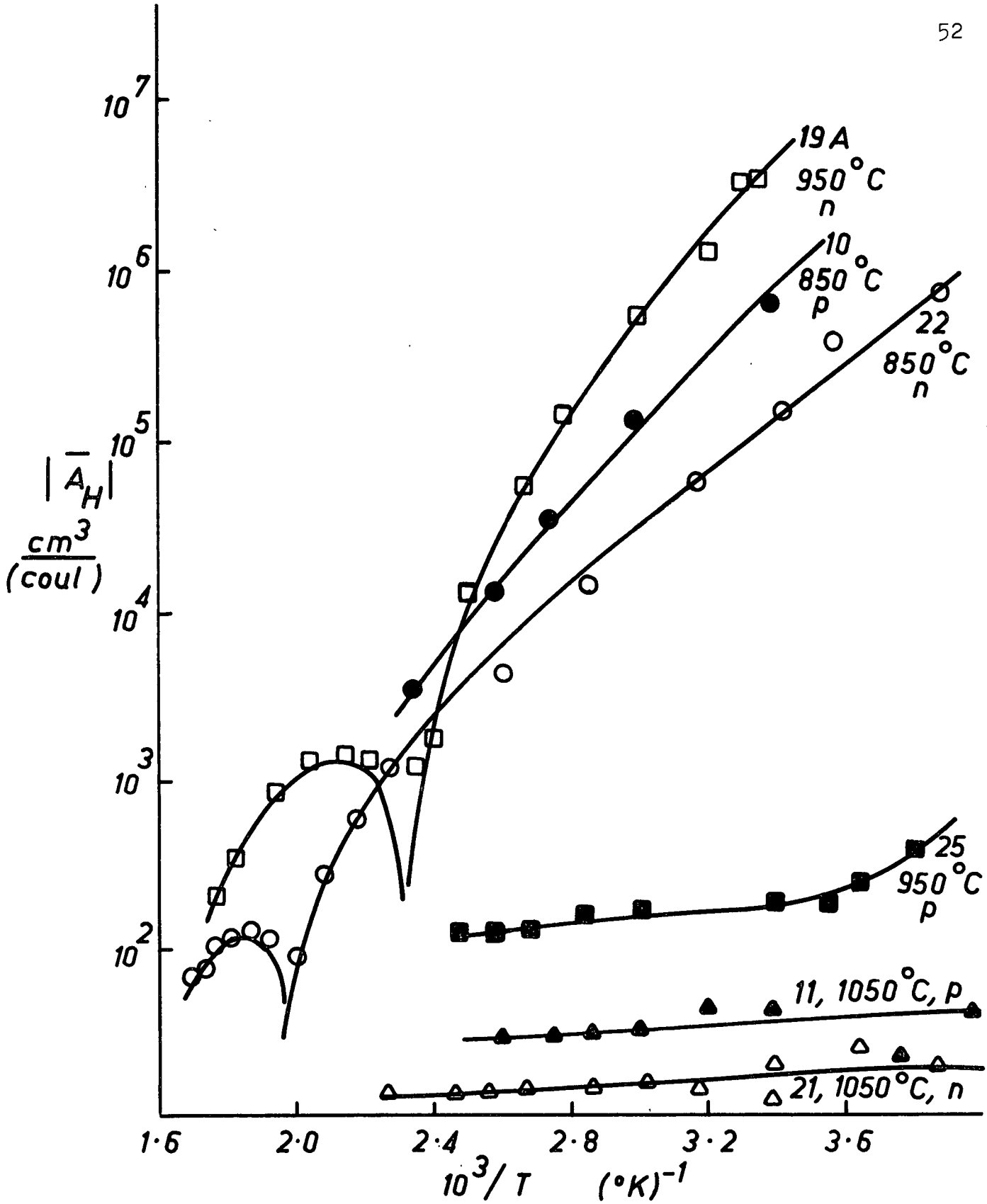

Figure 29 Hall Coefficient vs. Temperature of Films Deposited on to 0° Sapphire at Various Temperatures from n and p type Sources

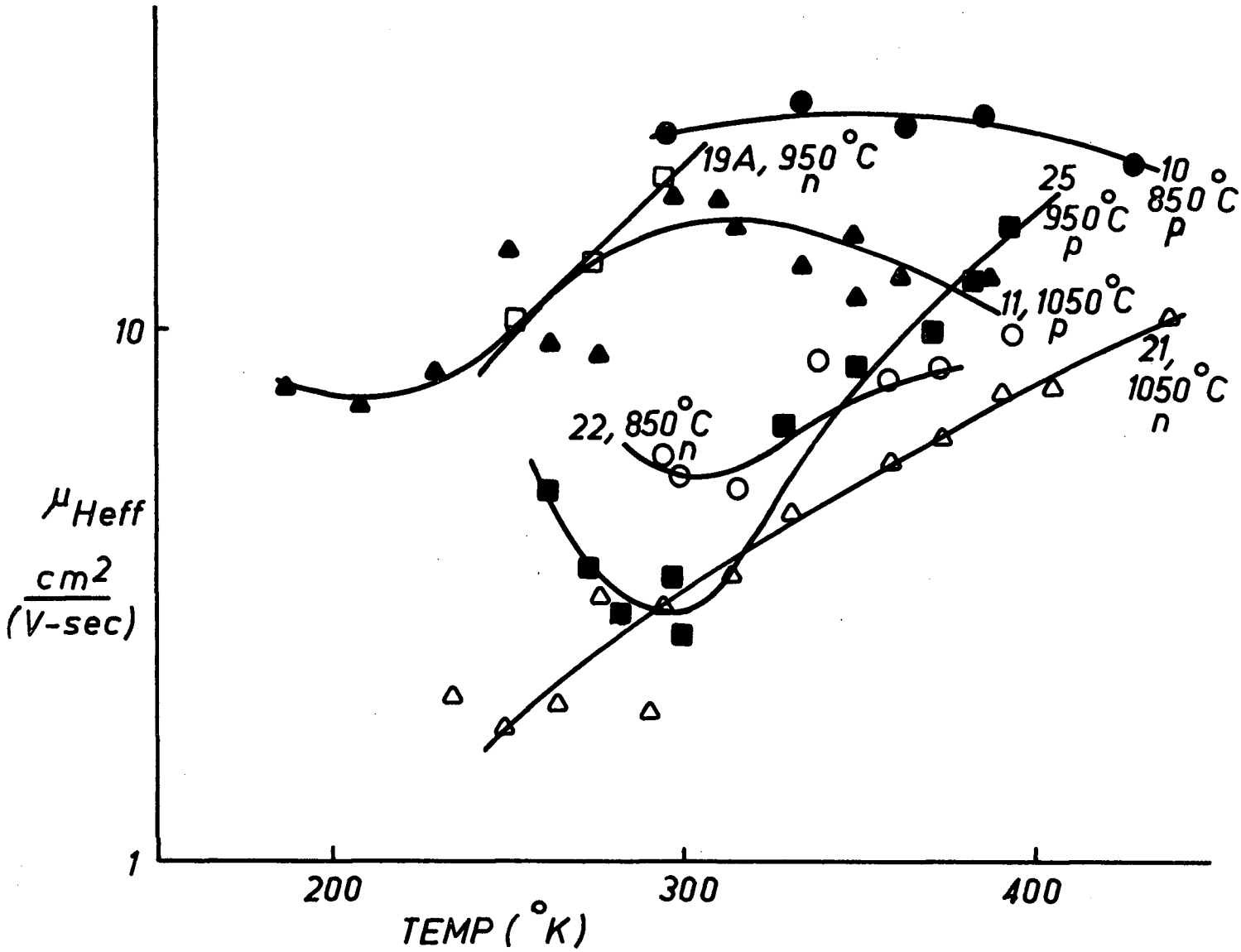

Figure 30 Hall Mobility vs. Temperature for Films Deposited on to C° Sapphire at Various Temperatures from n and p type Sources

This is because the high concentration of defects in both films swamps the effect of the dopant. Also the high concentration of defects in the crystallites probably results in a resistivity and hole concentration in crystallites not greatly different from those in the grain boundaries. Substituting $\rho_1 = \rho_2$ into equation 2.24 yields

$$\bar{\rho} = \rho_2 \,. \qquad 5.3$$

Substituting $A_{H1} = A_{H2}$ and $\rho_1 = \rho_2$ into equation 2.32 yields

$$\bar{A}_H = \frac{1}{p_2 q} \qquad 5.4$$

The Hall mobility, therefore, is

$$\mu_{Heff} = \mu_2 \qquad 5.5$$

The values of p_2 and μ_2 thus obtained are taken to be the values of hole concentration and mobility in the grain boundaries of films deposited at other than 850°C. This is reasonable since there is a high concentration of defects in the grain boundaries of most films in this study, regardless of deposition conditions. As shown in Figure 29 the Hall coefficient of the specimen deposited at 850°C from a p type source is larger (indicating a smaller hole concentration) than that of the specimen deposited at the same temperature from an n type source. This anomaly is probably due to spurious effects such as temperature gradients in the substrate during deposition or impurities in one of the films. The resulting Hall mobilities are also anomalous.

The film deposited at 950°C from an n type source had a resistivity at room temperature 3×10^3 times greater than

that deposited from a p type source at the same temperature. The specimen deposited from the n type source at 950°C (19A) had few defects (as indicated in the electron diffraction pattern in Figure 22) and, therefore, its resistivity is given by $\rho = \rho_2 \frac{l_1 + l_2}{l_2}$ (as explained in section 5.2). Using $l_1 = 4l_2$ (as obtained from Figure 20) and ρ_2 (as obtained for the specimens deposited at 850°C) the resistivity calculated for this specimen (19A) is shown in Figure 28 to match the experimental resistivity within 30% in the extrinsic range. The Hall coefficient of specimens deposited at 950°C is very dependent on the source dopant. The specimen made from the p type source (25) had a Hall coefficient very similar to that of the source material. This is expected since the electron diffraction pattern of this specimen was very similar to that of bulk material. The specimen made from the n type source (19A), on the other hand, exhibited a Hall coefficient characteristic of very heavily compensated material. Apparently the amount of n type dopant from the source was not sufficient to make the film n type. It did, however, tend to compensate the effect of defects which made the film p type.

Both specimens deposited at 1050°C from n and p type sources had very low Hall coefficients (therefore very high hole concentrations). This high hole concentration is expected for the film made from a p type source but is not expected for the film made from an n type source. This odd behaviour must be the result of aluminum atoms migrating from the Al_2O_3 substrate and doping the film p type. Such doping by aluminum

atoms appeared to be significant only in films deposited at 1050°C. Doping of silicon films on sapphire has also been observed by Ettner (1965) and by Dumin and Robinson (1966).

5.4 Effect of the Nature of the Substrate

5.4.1 Substrate Orientation (Al_2O_3)

The electron diffraction patterns in section 4.5 show that a film deposited on 0° sapphire had fewer defects than a film deposited on 60° sapphire at the same temperature. This resulted in a higher hole concentration (as shown in Figure 32) in films deposited on to 0° sapphire than in films deposited at the same temperature on to 60° sapphire. At the lowest temperature of deposition (850°C) the difference is slight. This is presumably because both films have large defect concentrations regardless of substrate-overgrowth misfits as indicated in the electron diffraction patterns of section 4.4.

The hole concentration and conductivity of films deposited on to 0° and 60° sapphire at a higher temperature (950°C) are very dependent on substrate orientation. The larger concentration of defects observed in the films deposited on 60° sapphire explains the lower hole concentration and conductivity. In films deposited at 950°C and and 1050°C from a p type source it is

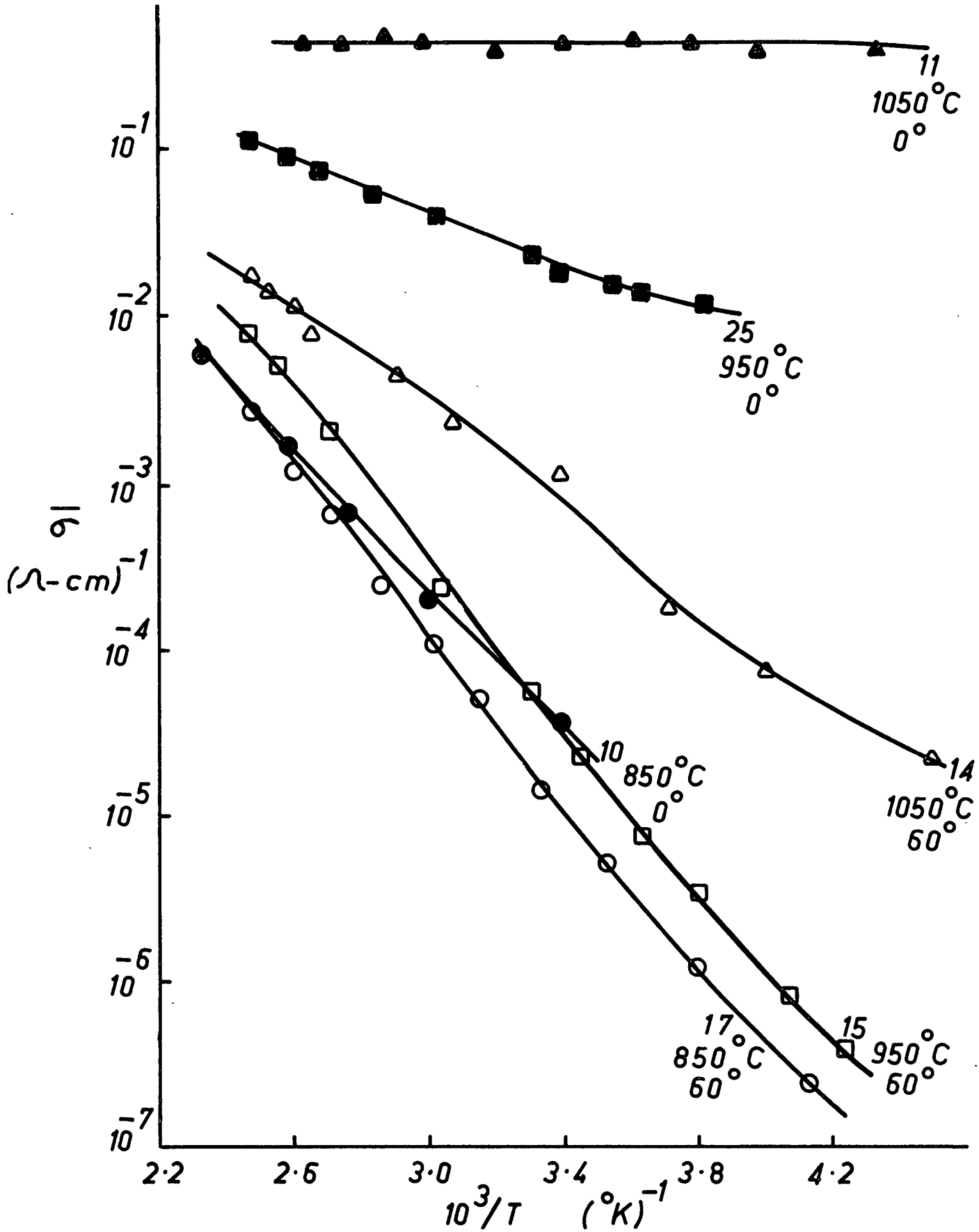

Figure 31 Conductivity vs. Temperature for Films Deposited on to 0° and 60° Sapphire at Various Temperatures From a p type Source

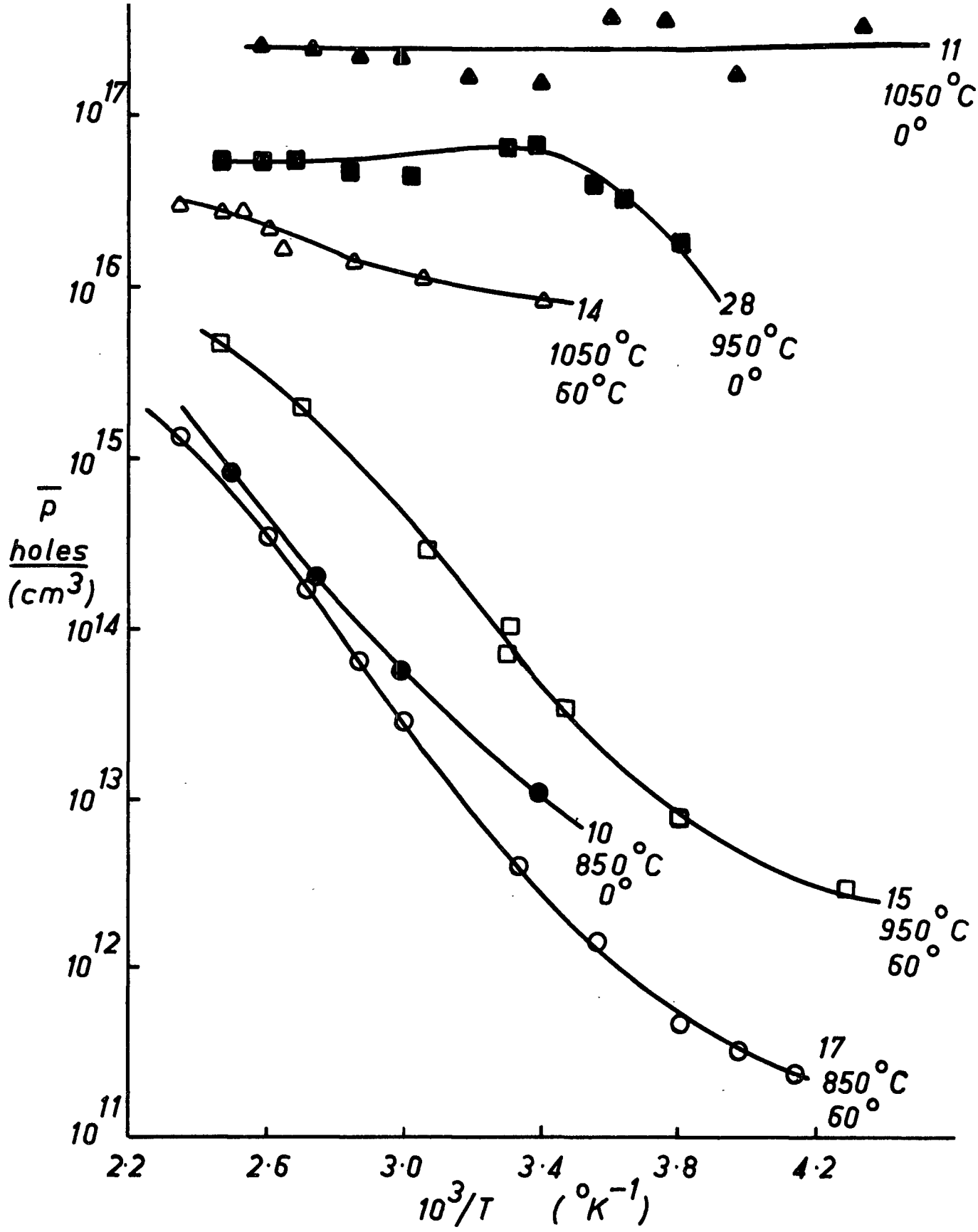

Figure 32 Hole Concentration vs. Temperature for Films Deposited on to 0° and 60° Sapphire at Various Temperatures from a p type Source

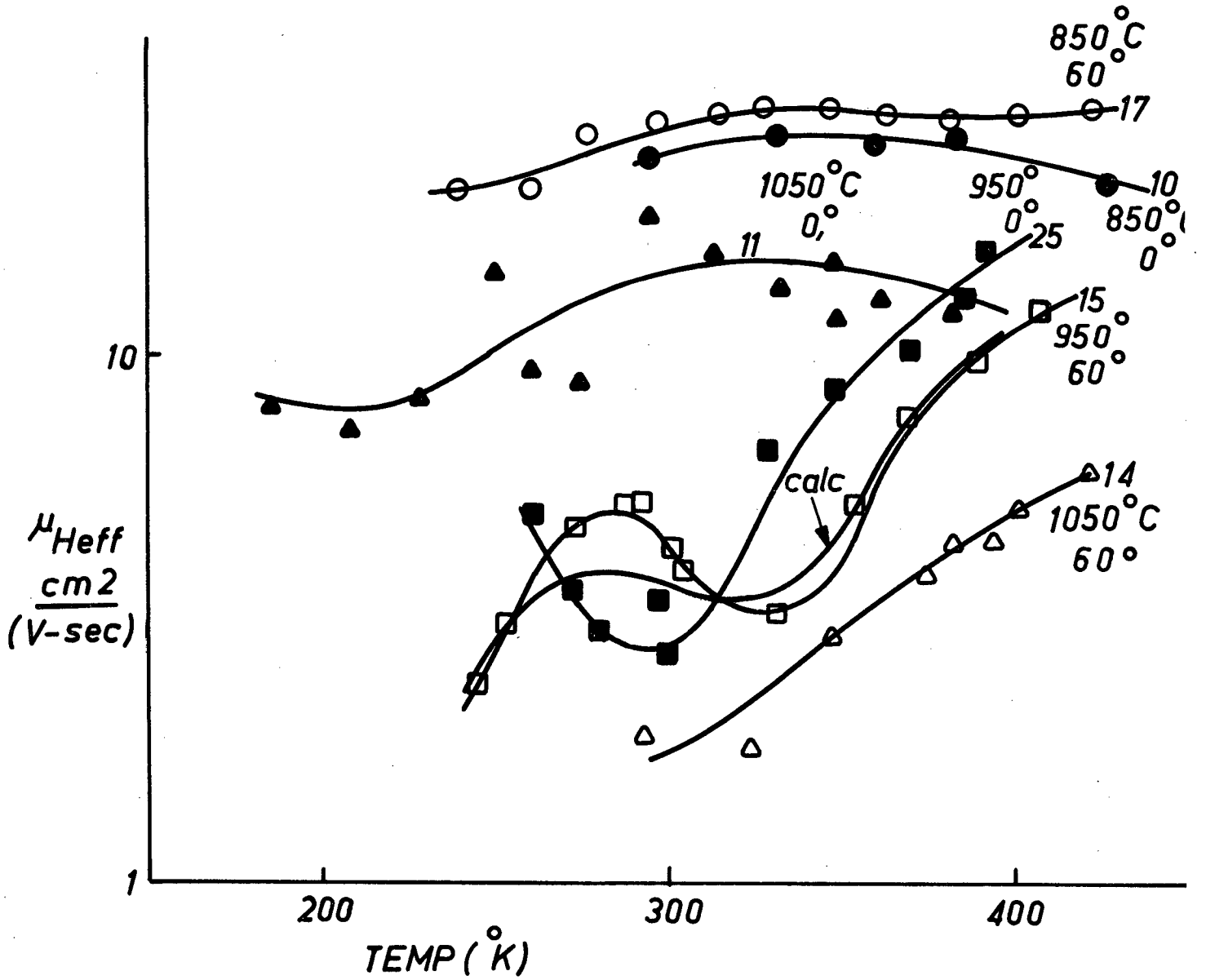

Figure 33 Hall Mobility vs. Temperature for Films Deposited on to 0° and 60° Sapphire at Various Temperatures from a p type Source

expected that $p_1 > p_2$ and $\mu_1 > \mu_2$. For the specimen deposited at 950°C on to 60° sapphire from the p type source (specimen 15) substituting $\rho_1 \ll \rho_2 \frac{l_2}{l_1}$ (where $l_1 = 4l_2$) into equations 2.24 and 2.32 yields

$$\bar{\rho} = \rho_2 l_2 / l_1 \qquad 5.7$$

and

$$A_H = A_{H1} + (1 + c)A_{H2}(l_2/l_1)^2 \qquad 5.8$$

where $c \simeq 0$ in the case of $\rho_1 \ll \rho_2$.

Although $A_{H1} > A_{H2}$ it is probably safe to assume that $A_{H1} \ll (\frac{l_2}{l_1})^2 A_{H2}$. Therefore the Hall coefficient becomes

$$A_H = A_{H1} = \frac{1}{p_1 q} \qquad 5.9$$

The Hall mobility is

$$\mu_{Heff} = \frac{l_1}{l_2} \frac{p_2}{p_1} \mu_2 \qquad 5.10$$

The values of p_2 and μ_2 obtained previously should not have changed a great deal with the increase in temperature of deposition. This is because a high concentration of defects is still present in the grain boundaries. By substituting these values of p_2 and μ_2 and the value of p_1 obtained from equation 5.9 into equation 5.10 the Hall mobility can be calculated. This calculated Hall mobility is shown in Figure 33 plot 15 to match the experimental Hall mobility very closely, even matching the peculiar negative slope portion of the curve. This negative slope appears to be the result of p_2 decreasing with temperature more rapidly than p_1.

With the exclusion of the specimen deposited on 0° sapphire at 1050°C (specimen 11), the Hall mobilities decreased with increasing temperature of deposition as shown in Figure 33. This is a very surprising result since it might be expected that the mobility would increase with increasing temperature of deposition because of the increasing perfection of the film. As indicated above the Hall mobility for films deposited at 950°C and 1050°C from a p type source is

$$\mu_{Heff} = \frac{l_1}{l_2} \frac{p_2}{p_1} \mu_2 \qquad 5.10$$

(This assumes that $l_1 \gg l_2$ and $\rho_1 \ll \frac{l_2}{l_1} \rho_2$.) The grain boundary hole concentration and mobility (p_2 and μ_2) are independent of the deposition temperature since the concentration of defects is high at the grain boundaries regardless of deposition temperature. The increase in l_1/l_2 with temperature of deposition is more than offset by the increase in p_1. Therefore, there is a decrease in the Hall mobility as indicated by equation 5.10. The high value of Hall mobility shown for specimen 11 is probably caused by significant doping of the grain boundary regions with aluminum atoms from the substrate.

5.4.2 Other Substrate Materials

Silicon was deposited on to a calcium fluoride substrate at 950°C. The resulting film was brown in colour (rather than dull to metallic grey as were the films deposited on sapphire) and peeled off the substrate easily. This apparent reaction between silicon and calcium fluoride at elevated temperatures

makes fluorite an unsuitable substrate for silicon films.

Silicon was evaporated on to magnesium oxide at 950°C and 850°C. At 950°C no film was formed. Evidently the critical temperature of deposition is considerably lower for magnesium oxide than for sapphire. At 850°C the film yielded a ring-type diffraction pattern characteristic of polycrystalline, disoriented films. Since the range of deposition temperatures between the temperature which produces polycrystalline films and the critical temperature is much less for magnesium oxide than for sapphire, the former is considered to be a less desirable substrate for silicon films than the latter.

5.5 Reproducibility of Electrical Properties

Figures 34, 35, 36, and 37 show the electrical properties of two films made under as nearly identical conditions as possible on 60° sapphire at 950°C. The hole concentration and conductivity plots indicate a maximum of 50% difference in these properties for the two films. There is a maximum difference of 100% in the Hall mobility in the two films. As indicated in section 5.4, the Hall mobility, in this case, is given by

$$\mu_{Heff} = \frac{l_1}{l_2} \frac{p_2}{p_1} \mu_2 \qquad 5.10$$

The relatively large difference in Hall mobility for the two films is the result of an accumulation of difference in $\frac{l_1}{l_2}$ and $\frac{p_2}{p_1}$ for the two films.

The electron diffraction patterns shown in Figure 37 indicate that both films had a fairly high concentration of

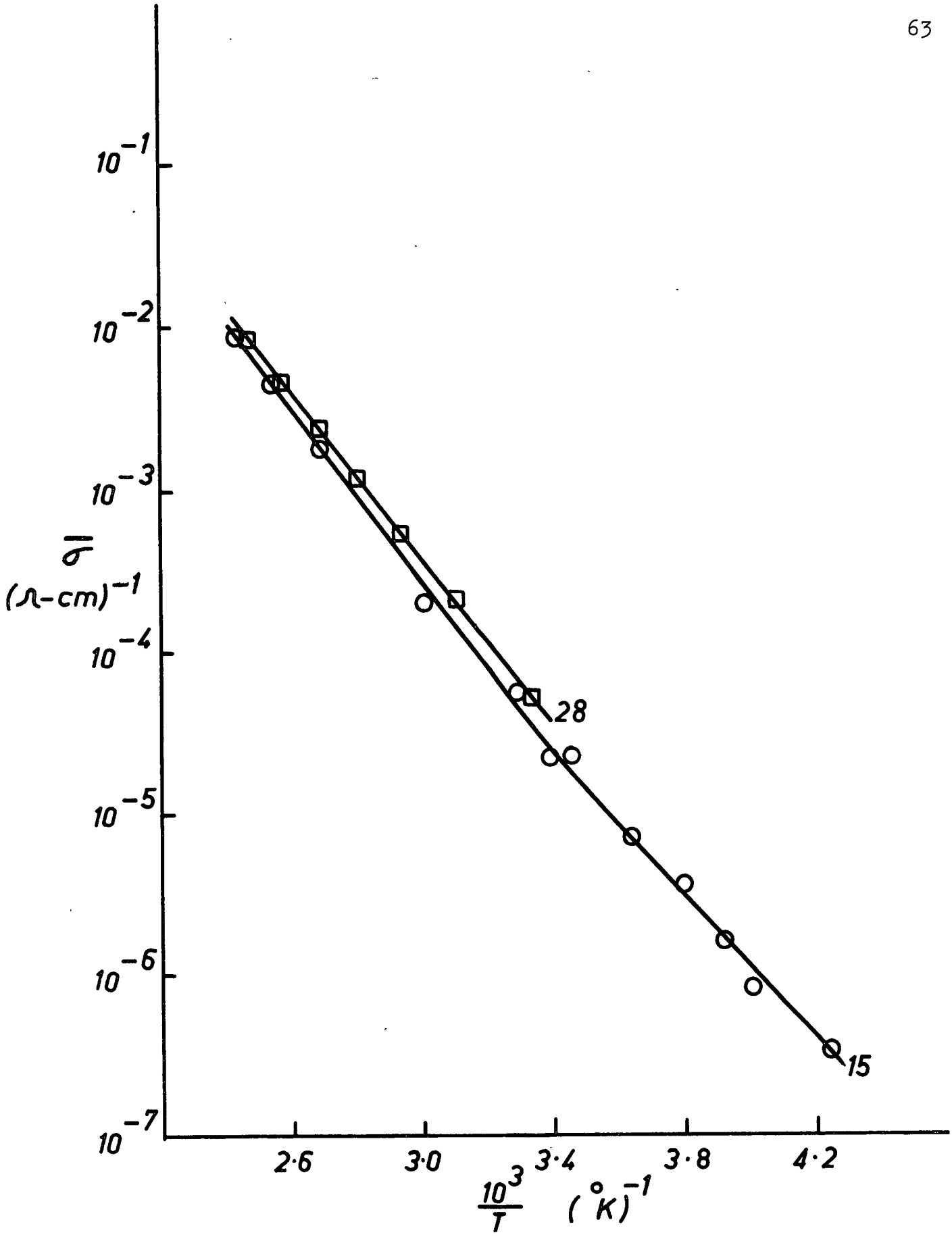

Figure 34 Conductivity vs. Temperature for Two Films Deposited on to 60° Sapphire at 950°C from a p type Source

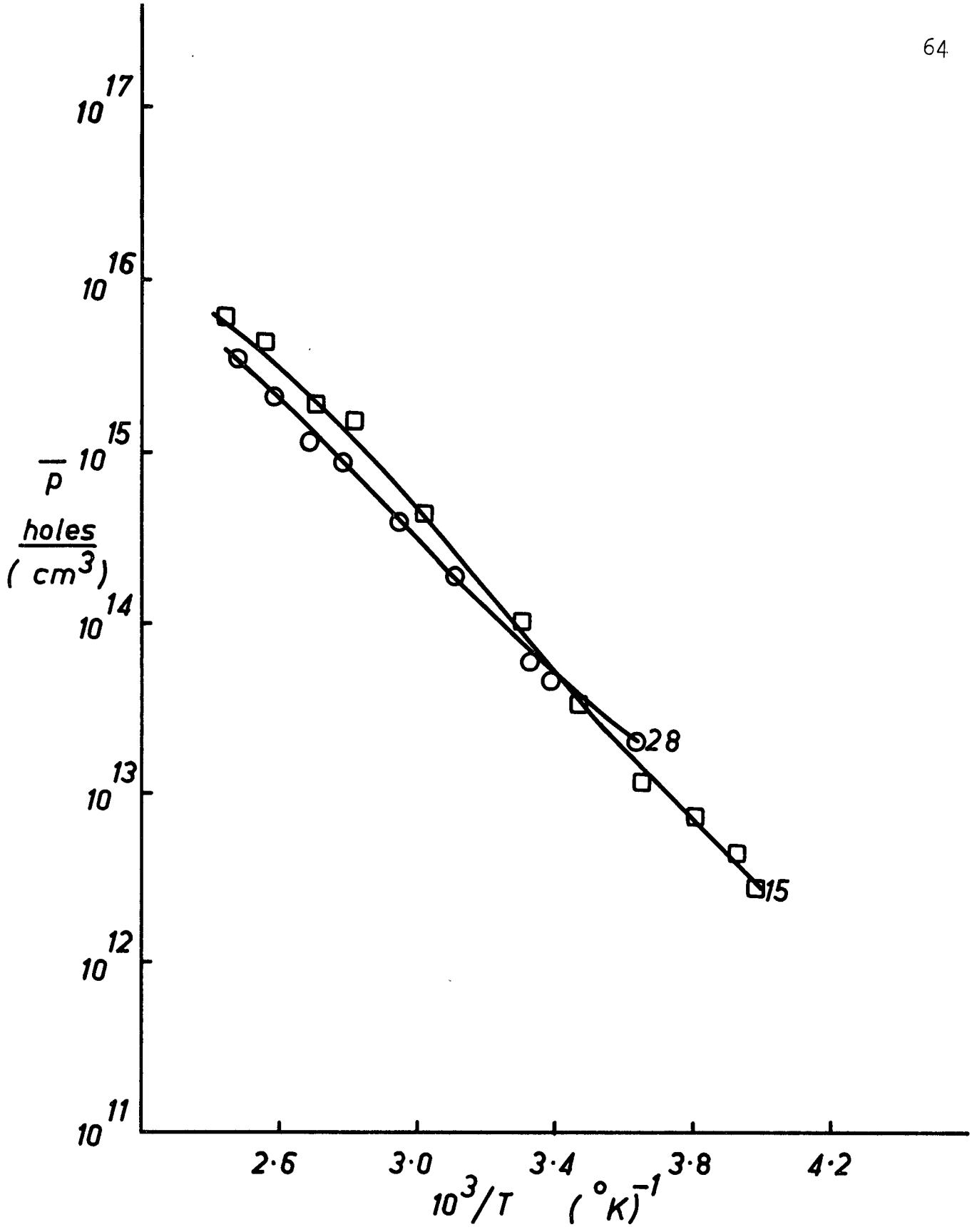

Figure 35 Hole Concentration vs. Temperature for Two Films Deposited on to 60° Sapphire at 950°C from a p type Source

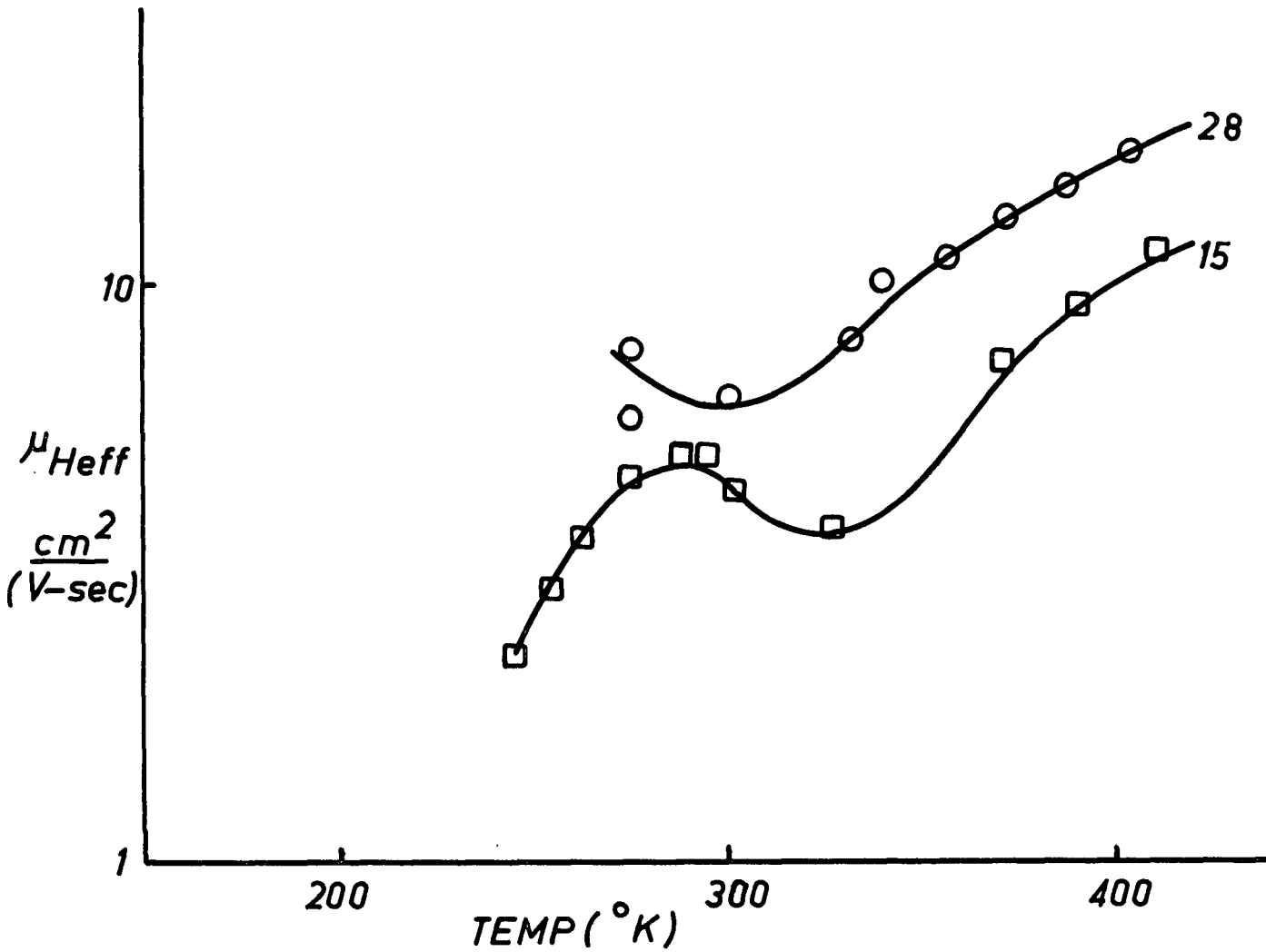

Figure 36 Hall Mobility vs. Temperature for Two Films Deposited on to 60° Sapphire at 950°C from a p type Source

defects. Specimen 28 appeared to possess a greater concentration of defects, which may account for the slightly lower hole concentration in the crystallite regions and, therefore, the slightly larger Hall mobility

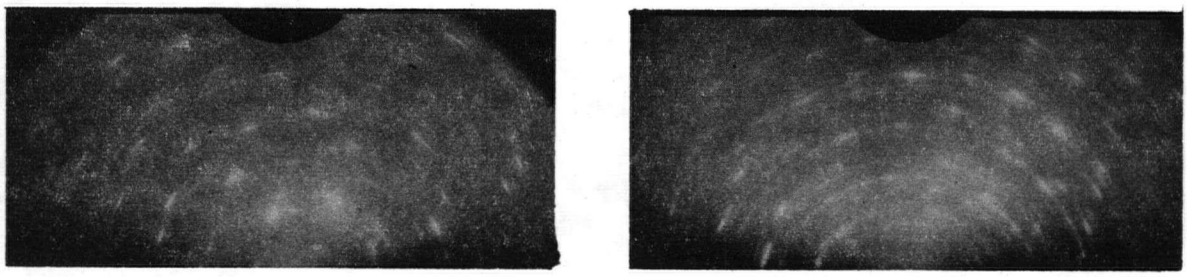

(a) Specimen 15 (b) Specimen 28

Figure 37 Electron Diffraction Patterns of Two Films Deposited at 950°C on 60° Sapphire.

5.6 Homogeneity of Films

The electrical properties of all three specimens on one substrate were examined to determine the uniformity of the film. Specimen 19 was chosen for this study because it was deposited on 0° sapphire. It is expected that a temperature gradient in a 0° oriented sapphire will have a greater effect on the electrical properties of the film than the same temperature gradient in a 60° oriented sapphire. In addition, the doping from the substrate is more readily distinguished from doping by the source for specimen 19 than for any other specimen.

The maximum temperature difference between points on the substrate during deposition was estimated at 20°C. The temperature gradient appears to have caused a factor of 5 difference in the macroscopic conductivity of specimens on

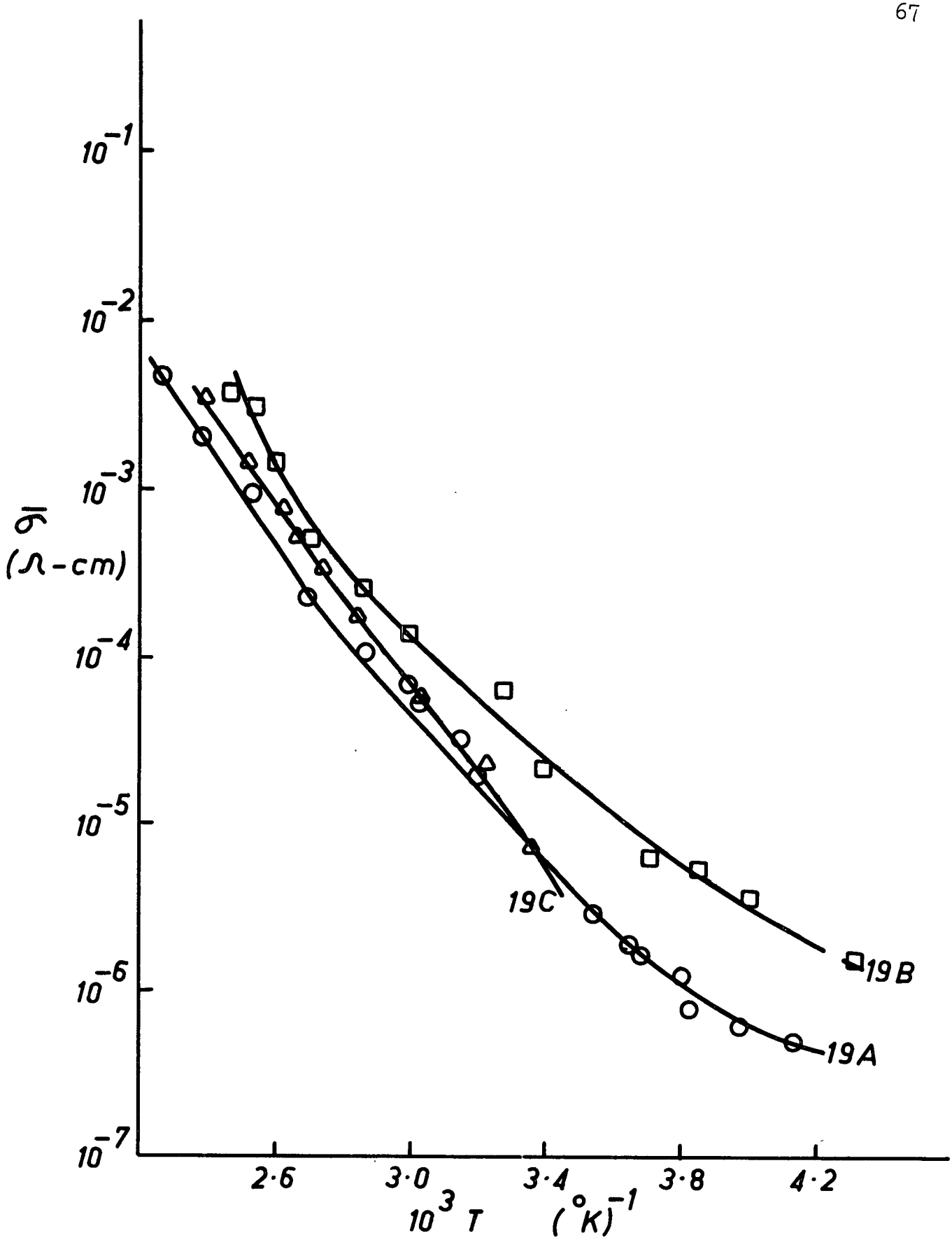

Figure 38 Conductivity vs. Temperature for Three Specimens Deposited on to a 0° Sapphire substrate at 950°C from an n type Source

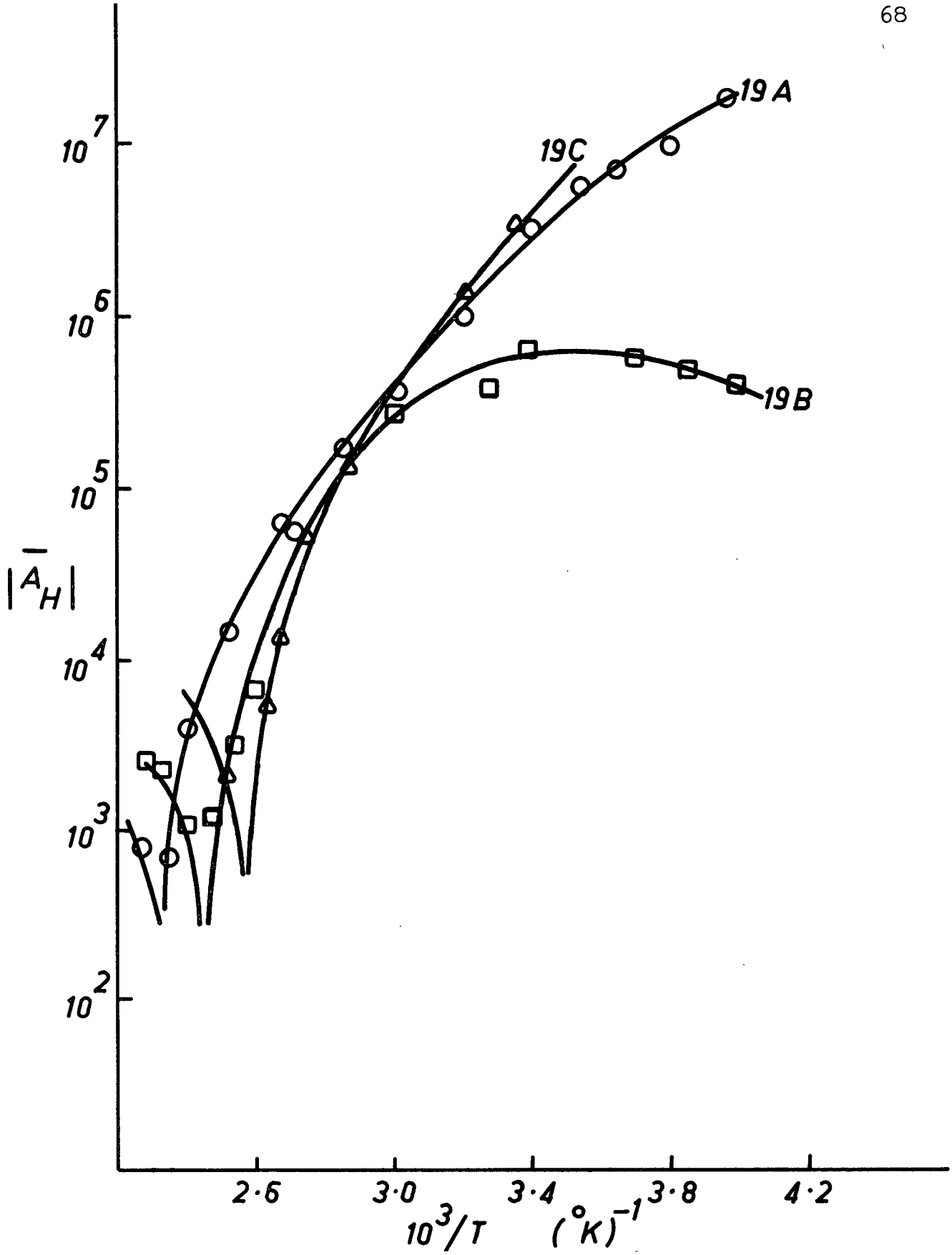

Figure 39 Hall Coefficient vs. Temperature for Three Specimens Deposited on to a 0° Sapphire Substrate at 950°C from an n type Source

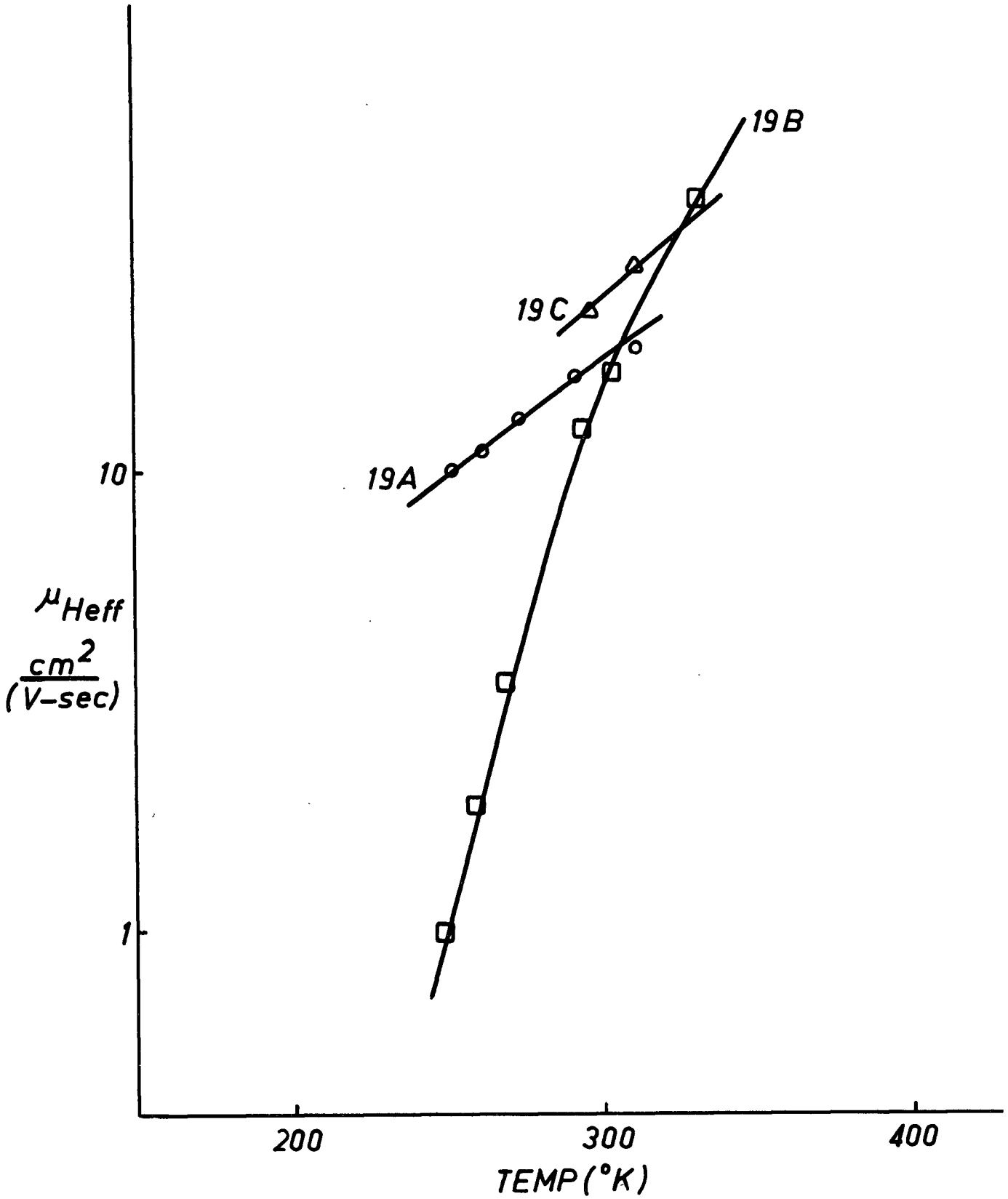

Figure 40 Hall Mobility vs. Temperature for Three Specimens Deposited on to a 0° Sapphire Substrate at 950° from an n type Source

substrate 19 (as shown in Figure 38).

The variation of the Hall coefficient with temperature is shown in Figure 39. All three specimens changed sign from positive to negative at high temperatures. Specimen 19B exhibited an "exhaustion" region for temperatures below 300°K. The radically different slope in Hall mobility for specimen 19B is a result of the "exhaustion" range in $\bar{p}$.

6. CONCLUSIONS

The growth of silicon films occurred by the formation of nuclei which subsequently grew together to form a continuous film. Crystallites grew larger and more oriented with increasing film thickness. In addition, the crystallites became larger and more oriented with increasing temperature of deposition. A critical temperature of deposition was observed above which no silicon deposited. A few degrees below this temperature nucleation occurred more readily at microscratches on the substrate than on smooth portions of the substrate. The crystallites grown on 0° sapphire were larger and more oriented than those grown on 60° sapphire.

All silicon films studied were p type at room temperature, even those fabricated from a 1.0Ω-cm n type source. Films produced from this heavily doped n type silicon exhibited intrinsic behaviour at considerably lower temperature than those produced from p type silicon. Since this behaviour is evidence that the n type dopant does evaporate and deposit with the silicon, it is speculated that n type films could be produced from a block of silicon which is very heavily n type doped.

The low hole concentration of films deposited at $850^{\circ}C$ is characteristic of very heavy compensation of acceptor and donor levels. All films deposited on 60° oriented sapphire exhibited compensation to some degree regardless of the temperature of deposition (up to $1050^{\circ}C$). Films deposited on sapphire substrates at low temperatures ($850^{\circ}C$) exhibited no exhaustion range of temperature. This is the result of several acceptor

levels being present in the energy band. With increasing temperature, progressive levels are ionized giving rise to a fairly steady increase in hole concentration with temperature. The film deposited on 0^{o} oriented sapphire at $950^{o}C$ from a p type source exhibited an exhaustion region in the hole concentration but not in the resistivity. This is explained in terms of the inhomogeneous film model in that the resistivity of this specimen was governed by the grain boundaries while the Hall coefficient was determined by the crystallites. The similarity in behaviour of this specimen to that of bulk material was expected because the electron diffraction patterns indicated few defects.

For deposition at $1050^{o}C$ evidence was presented that aluminum atoms diffused from the substrate into the silicon film and caused p type doping which swamped the effect of the source dopant. Such doping from the substrate had considerably greater effect on the electrical properties of films deposited on 0^{o} oriented sapphire than on films deposited on to 60^{o} oriented sapphire because the 60^{o} specimens had greater defect concentrations than the 0^{o} specimens.

APPENDIX I

THE VAN DER PAUW CONFIGURATION

For a thin Hall specimen of arbitrary periphery (as shown in Figure A1) van der Pauw proved that the resistivity is given by

$$\rho = \frac{\pi t}{2 \ln 2} \left(R_{AB,CD} + R_{BC,DA}\right) f\left(\frac{R_{AB,CD}}{R_{BC,DA}}\right) \quad \text{(esu)}$$

where

$$R_{AB,CD} = \frac{V_D - V_C}{I_{AB}} \qquad \text{and} \qquad R_{BC,DA} = \frac{V_D - V_A}{I_{BC}}$$

and the function $f\left(\frac{R_{AB,CD}}{R_{BC,DA}}\right)$ is given in Figure A2.

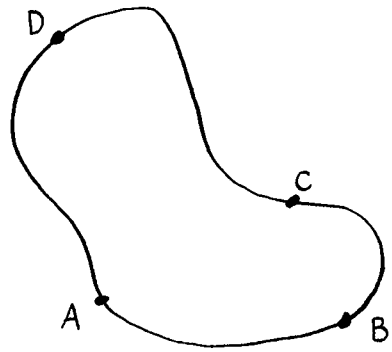

Figure A1

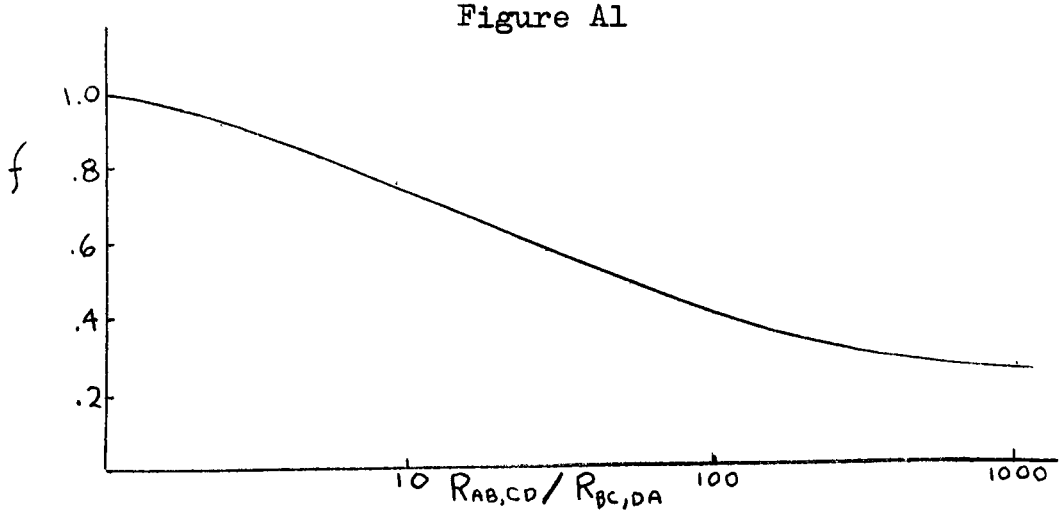

Figure A2

When a magnetic field is applied perpendicularly to the specimen, a Hall voltage given by

$$V_H = \frac{10^{-8} A_H B I}{t} \quad \text{(esu)}$$

is developed perpendicularly to the direction of current flow and also perpendicularly to the magnetic field.

REFERENCES

1. Albert, M.P. and Combs, J.F., "Thickness Measurements of Epitaxial Films by the Infrared Interference Method," J. Electrochem. Soc., Vol. 109, pp. 709-712, 1962.

2. Bardeen, J., and Pearson, G.L., "Electrical Properties of Pure Silicon and Silicon Alloys Containing Boron and Phosphorus," Phys. Rev., Vol. 75, pp. 865-883, March 1949.

3. Bicknell, R.W., Charig, J.M., Joyce, B.A., and Stirland, D.V., "The Epitaxial Deposition of Silicon on Quartz," Phil. Mag., Vol. 9, pp. 965-978, June, 1964.

4. Booker, G.R., and Unvala, B.A., "Growth of Epitaxial Silicon Layers by Vacuum Evaporation I," Phil. Mag., Vol. 102, pp. 691-701, April, 1964.

5. Booker, G.R., and Unvala, B.A., "Growth of Epitaxial Silicon Layers by Vacuum Evaporation II", Phil. Mag., Vol. 103, pp. 10-30, January, 1965.

6. Conwell, E.M., and Weisskopf, V.F., "Theory of Impurity Scattering in Semiconductors", Phys. Rev., Vol. 69A, p. 258, 1946.

7. Crawford, J.H., and Clelland, J.W., Progress in Semiconductors ed. A.F. Gibson, Vol. 2, Heywood and Co., London, 1957, pp. 67-108.

8. Dexter, D.L., and Seitz, F., "Effects of Dislocations on Mobilities in Semiconductos", Phys. Rev., Vol. 86, pp. 964-965, 1952.

9. Doo, V.Y., "Thin Silicon Film Growth on Polycrystalline Alumina Ceramic", J. Electrochem. Soc., Vol. 111, pp. 1196-1198, 1964.

10. Dumin, D.J., and Robinson, P.H., "Autodoping of Silicon Films Grown Epitaxially on Sapphire", J. Electrochem. Soc., Vol. 113, pp. 469-472, 1966.

11. Ettner, P.J., Paper presented at the Conf. on Non-metallic Films, Chelsea, Sept., 1965.

12. Grübaum, E., and Mitchell, J.W., "The Observation of Interfacial Dislocations in Nickel Bromide Grown Epitaxially on Thin Chromic Bromide Crystals," Single Crystal Films, eds. M.H. Francombe and H. Sato, Pergamon Press, New York, 1963.

13. Handelman, E.T., and Dovilonis, E.I., "Epitaxial Growth of Silicon by Vacuum Sublimation," J. Electrochem. Soc., Vol. 111, pp. 201-206, 1964.

14. Johnson, V.A., and Lark-Horowitz, K., "Transition from Classical to Quantum Statistics in Germanium Semiconductors at Low Temperatures", Phys. Rev., Vol. 71, pp. 374-375, March, 1947a.

15. Johnson, V.A. and Lark-Horowitz, K., "Theory of Low Temperature Semiconductor Resistivity," Phys. Rev., Vol. 72, pp. 531, Sept., 1947b.

16. Kataoka, Y., "Some Properties of Evaporated Silicon Films," J. Phys. Soc. of Japan, Vol. 17, pp. 967-969, June, 1962.

17. Manasevit, H.M., and Simpson, W.I., "Single Crystal Silicon on Sapphire Substrate," J. Appl. Phys., Vol. 35, pp. 1349-1351, April, 1964.

18. Many, A., Goldstein, Y., and Grouver, N.B., "Semiconductor Surfaces," J. Wiley and Sons Inc., New York, 1965.

19. Matthews, J.W., "The Observation of Dislocations to Accommodate the Misfit between Crystals with Different Lattice Parameters", Phil. Mag., Vol. 6, pp. 1347-1349, 1961.

20. Matthews, J.W., "The Observation of Dislocations to Accommodate the Misfit between Slightly Different Gold-Palladium Alloys", Single Crystal Films, eds., M.H. Francombe and H. Sato, Pergamon Press, New York, 1963, pp. 165-172.

21. McAleer, W.J., Pollak, P.I., and Kollmann, H., "Polycrystalline Silicon Films on Foreign Substrates," J. Electrochem. Soc., Vol. 111, pp. 877-878, 1964.

22. Mendelsson, S., "Growth and Imperfections in Epitaxially Grown Silicon on Variously Oriented Silicon Substrates", Single Crystal Films, eds., M.H. Francombe and H. Sato, Pergamon Press, New York, 1963, pp. 251-280.

23. Morin, F.J., and Maita, J.P., "Electrical Properties of Silicon Containing Arsenic and Boron," Phys. Rev., Vol. 96, pp. 28-25, Oct., 1954.

24. Pashley, D.W., "The Nucleation, Growth, Structure, and Epitaxy of Thin Surface Films," Advances in Physics, Vol. 14, pp. 327-416, July, 1965.

25. Pinsker, Z.G., "Electron Diffraction", Butterworth Scientific Pubs., London, 1953.

26. Putley, E.H., "The Hall Effect and Related Phenomena," Butterworth Scientific Pubs., London, 1960.

27. Read, W.T., "Statistics of the Occupation of Dislocation Acceptor Centers," Phil. Mag., Vol. 45, pp. 119-1128, 1954.

28. Read, W.T., "Scattering of Electrons by Charged Dislocations in Semiconductors," Phil. Mag., Vol. 46, pp. 111-131, 1955.

29. Rhodin, T.N., and Walton, D., "Nucleation of Oriented Films," Single Crystal Films, eds., M.H. Francombe and H. Sato, Pergamon Press, New York, 1963, pp. 31-41.

30. Salama, C.A.T., Ph.D. Thesis, University of British Columbia, Vancouver, 1966.

31. Shockley, W., "Electrons and Holes in Semiconductors," D. Van Nostrand Inc., New York, 1950.

32. Shockley, W., and Bardeen, J., "Energy Bands and Mobilities in Monatomic Semiconductor," Phys. Rev., Vol. 77, pp. 407-408, 1950a.

33. Shockley, W., and Bardeen, J., "Deformation Potentials and Mobilities in Non-polar Crystals", Phys. Rev., Vol. 80, pp. 72-80, Oct., 1950b.

34. Sloope, B.W., and Tiller, C.O., "Formation Conditions Structure, and Electrical Properties of Germanium Films Deposited on Single Crystal Substrates," Trans. of Tenth Nat. Vac. Symp., Macmillan and Co., New York, 1963, pp. 339-347.

35. Smith, R.A., "Semiconductors", Cambridge University Press, Cambridge, 1964.

36. Spenke, E., "Electronic Semiconductors", McGraw-Hill, New York, 1958.

37. Thompson, G.P., and Cochrane, W., "Theory and Practice of Electron Diffraction", Macmillan and Co., London, 1939.

38. van Daal, H.J., "Mobility of Charge Carriers in Silicon Carbide," Philips Research Report Supplement, 1965.

39. van der Merwe, J.H., "Interfacial Misfit and Bonding between Oriented Films and Their Substrates," Single Crystal Films, eds. M.H. Francombe and H. Sato, Pergamon Press, New York, 1964.

40. van der Pauw, L.V., "A Method of Measuring Specific Resistivity and Hall Effect of Discs of Arbitrary Shape," Philips Research Reports, Vol. 13, pp. 1-9, February, 1958.

41. Vavilou, V.S., "Effects of Radiation on Semiconductors," Consultants Bureau, New York, 1965.

42. Volger, J., "Note on the Hall Potential Across on Inhomogeneous Conductor," Phys. Rev., Vol. 79, pp. 1023-1024, Sept., 1950.

43. Widmer, H., "Epitaxial Growth of Silicon Films on Silicon in Ultra High Vacuum," Appl. Phys. Lett., Vol. 5, pp. 108-110, Sept., 1964.

44. Ziman, J.M., "Electrons and Phonons", Oxford University Press, London, 1963.